VERSATILITY OF M13 BACTERIOPHAGE IN MEDICINE:

VACCINE STORAGE AND CANCER DIAGNOSTICS

by

Amy Shi

B.S., Chemical Engineering (2004)

Massachusetts Institute of Technology

SUBMITTED TO DEPARTMENT OF MATERIALS SCIENCE AND ENGINEERING IN PARTIAL
FULFILLMENT OF THE REQUIREMENTS FOR THE DEGREE OF

MASTER OF SCIENCE IN MATERIALS SCIENCE AND ENGINEERING
AT THE
MASSACHUSETTS INSTITUTE OF TECHNOLOGY

FEBRUARY 2007

Signature of Author: _____
Department of Materials Science and Engineering
January 19, 2007

Certified by: _____
Angela M. Belcher
Professor of Materials Science and Engineering
Thesis Supervisor

Accepted by: _____
Samuel M. Allen
POSCO Professor of Physical Metallurgy
Chairman, Department Committee on Graduate Students

VERSATILITY OF M13 BACTERIOPHAGE IN MEDICINE: VACCINE STORAGE AND CANCER DIAGNOSTICS

By

Amy Shi

Submitted to Department of Materials Science and Engineering
On January 19, 2007 in Partial Fulfillment of the
Requirements for the Degree of Master of Science in
Materials Science and Engineering

ABSTRACT

Two novel ways of engineering the filamentous bacteriophage, M13, for the prevention, diagnosis, and treatment of human disease are proposed. Both ways are founded on the unique structural properties of the M13 bacteriophage and the ability of its major and minor coat proteins, p3 and p8, to be manipulated to serve as virus-based multifunctional platforms. The first project addresses the problem of vaccine storage and the cold chain (requirement to store vaccines at 2-8°C or lower). The need for refrigeration leads to high cost, difficult field delivery, and high potential for vaccine instability. By capitalizing on the liquid crystalline nature and unique diffraction patterns of phage films, we aim to encapsulate vaccines in a 3-D liquid crystalline matrix that would not only allow for stability at elevated temperatures but would also allow for easy detection of viability by using a laser light and noting the diffraction pattern. We chose luciferase as a model for a protein-based vaccine, and found several phage-borne peptide sequences with increased affinity to luciferase compared to controls. Two of these sequences, CKLHGTSRC and CTHKNQAC were chosen to form luciferase-encapsulated phage films. The second project addresses the need of more sensitive imaging techniques for early detection of cancer. M13 bacteriophage were used in combination with quantum dots and magnetic nanoparticles as bigger and brighter markers for cancer lesions. A 100% expressed p8 library was created for screening against potential cancer markers and work will soon proceed with screening against several cancer cell lines. In addition, a Type 83 phage was created that had a sequence directed against vascular cell adhesion molecule-1 (VCAM-1) expressed on the p3 and a tri-glutamate sequence (E3) on the p8 that could bind well to positively charge molecules like amines. Successful attachment of amine-terminated CdSe/ZnS quantum dots to p8E3 phage (E3 on p8 and wildtype on p3) was shown and III-V quantum dots (GaN and InN) were water solubilized for use *in vivo*. The goal is to combine all parts and start *in vivo* testing and screening, as well as to expand our cancer targeting repertoire.

Thesis Supervisor: Angela M. Belcher
Title: Professor of Materials Science and Engineering

ACKNOWLEDGEMENTS

I would first like to thank my advisor, Professor Angela Belcher for all her support. She has encouraged me to pursue my research interests, and has opened up opportunities for me to venture into various medical device areas, suggesting collaborations as well as new avenues of thinking and research. She has been of immense influence on me, sharing with me her creativity, inventiveness, and passion for science and technology. Watching her at work and being in this lab has been truly inspirational. A special thanks to my lab mates, who over the years have reached out to teach me many techniques, helped me flesh out research obstacles, and gave me an enriching intellectual environment.

I am also deeply grateful to my loving parents, Ying Lin and Shixiang Shi, for their support, and advice throughout my life, and especially during my graduate career. They have continuously provided wisdom as well as unconditional love and acceptance. They created in me a foundation for the love of learning and the desire to help people. They taught me to try my best no matter the outcome. When the road gets hard, knowing that family is always there for me takes a great burden off my shoulders.

I would like to thank my friends who have been there to laugh with me, cry with me, struggle through classes and qualifiers, and have been my stronghold in the past few years. Without their support and graciousness, graduate school life would not have been nearly as warm and fulfilling as it has been. And in particular, I can not imagine going through all the ups and down of research and graduate school in the past few years without the support of my best friend and partner, Jason. Thank you.

Lastly, my experience has taught me that research is a great game of chance. We can only control what we put into the pot, not what we get out. The same goes with life. "In the book of life every page has two sides: we human beings fill the upper side with our plans, hopes and wishes, but providence writes on the other side, and what it ordains is seldom our goal -- Nisami" And through it all, is a chance for us to grow, mature, and learn the meaning of Grace. Thank you God for this amazing opportunity!

TABLE OF CONTENTS

LIST OF TABLES 7

LIST OF FIGURES 8

CHAPTER 1 – INTRODUCTION 10

1.1 THESIS OVERVIEW 10
1.2 PHAGE BIOLOGY 10
1.3 PHAGE DISPLAY 14

CHAPTER 2 – VACCINE STORAGE SYSTEM BASED ON THE M13 BACTERIOPHAGE 16

2.1 ABSTRACT 16
2.2 INTRODUCTION 16
2.2.1 Vaccine Storage and Protein-Based Vaccines 16
2.2.2 M13 Bacteriophage as a Liquid Crystal 18
2.2.4 Stabilizing Vaccines within Liquid Crystalline Phage Films 21
2.2.3 Luciferase 22
2.3 METHODS, RESULTS, AND DISCUSSION 25
2.3.1 Overview 25
2.3.2 Luciferase 25
2.3.3 Biopanning 25
2.3.4 Enzyme Linked ImmunoSorbant Assay (ELISA) 30
2.3.5 Biopanning with Luciferin Competition in Every Round 32
2.3.7 ELISA of Selected High Affinity Clones 34
2.3.8 Large Scale Amplification 37
2.3.9 Luciferase Activity Assay Methods 38
2.3.10 M13 – Luciferase Films 39
2.4 CONCLUSIONS AND FUTURE WORK 41

CHAPTER 3 - VIRUS-BASED MULTIFUNCTIONAL PLATFORM FOR *IN VIVO* CANCER DIAGNOSTICS 42

3.1 ABSTRACT 42
3.2 INTRODUCTION 43
3.2.1 Phage in Medicine 43
3.2.2 Phage Advantages and Disadvantages for Cancer Diagnostics 46
3.2.3 Breast Cancer 47
3.2.4 Virus-Based Cancer Detection Platform 49
3.3 METHODS, RESULTS, AND DISCUSSION 51
3.3.1 Genetic Engineering of M13 Bacteriophage 51
3.3.1.1 Type 8 Phage Library (34) in collaboration with Soo-Kwan Lee 51
3.3.1.2 Type 83 Genetic Engineering in Collaboration with Chung-Yi Chiang 54
3.3.1.3 Type 8 Directed Genetic Engineering 56
3.3.2 Imaging Modalities 58
3.3.2.1 Quantum Dot Basics 58
3.3.2.2 Magnetic Nanoparticle Basics 61
3.3.2.3 Attaching CdSe/ZnS Quantum Dots to E3 Phage 62
3.3.2.4 Ways to Water Solubilize Nanoparticles 64
3.3.2.5 GaN and InN Quantum Dots (In collaboration with Dr. Jifa Qi) 65
3.4 CONCLUSIONS AND FUTURE WORK 73

CHAPTER 4 – SUMMARY AND CONCLUSIONS 75

APPENDIX A: BIOPANNING SEQUENCES 76

APPENDIX B: HUMAN PHAGE THERAPY REFERENCES 78

APPENDIX C: M13SK CONSTRUCTION 80

APPENDIX D: M13SK P8 LIBRARY CONSTRUCTION **82**
REFERENCES **88**

LIST OF TABLES

TABLE 1. PHAGE CONCENTRATIONS (PFU/µL) BIOPANS 1-3. ELUATE REFERS TO THE COLLECTED PHAGE AFTER PH ELUTION AND AMPLIFIED ELUATE REFERS TO PHAGE AFTER BEING AMPLIFIED IN *E.COLI* FOR 4.5 HOURS AT 37°C. 28
TABLE 2. CONCENTRATION OF PHAGE FOR ELISA OF PL3 WITH CONTROLS. 30
TABLE 3. TITERING RESULTS FROM BIOPAN ROUNDS 1B TO 4B....33
TABLE 4. PHAGE CLONES SELECTED FOR AMPLIFICATION FOR ELISA. PHAGE CLONES WERE SELECTED BASED ON CONSENSUS IN DNA SEQUENCING RESULTS OR APPEARANCE IN MULTIPLE ROUNDS. 34
TABLE 5. CONCENTRATION OF AMPLIFIED PHAGE FOR ELISA (PFU/µL)....35
TABLE 6. TITER RESULTS FROM LARGE SCALE AMPLIFICATIONS OF CLONES 1 AND 3....37
TABLE 7. LUCIFERASE PHAGE FILM CONDITIONS AND SAMPLES....39
TABLE 8. EXAMPLES OF APPLICATIONS OF PHAGE THERAPY IN TECHNOLOGY AND MEDICINE. (45) 45
TABLE 9. EXAMPLE PEPTIDES FROM TYPE 8 M13 PHAGE LIBRARY....53
TABLE 10. DIFFERENT CONDITIONS OF WATER SOLUBILIZING GAN QUANTUM DOTS. 60MG OF GAN(CTAB) WAS ADDED TO 3 ML $CHCL_3$ AND DIVIDED INTO SIX AMINE SAMPLES. 14 MG DSPE-PEG(2000), 8 MG DPPC, AND 12 MG DSPE-PEG(2000)-AMINE WERE MIXED IN 2 ML $CHCL_3$ AND WERE DIVIDED INTO 4 SAMPLES. LASTLY, 6 MG DSPE-PEG(2000), 4 MG DPPC, AND 6 MG DSPE-PEG(2000)-COOH WERE MIXED IN 1 ML $CHCL_3$ AND DIVIDED BETWEEN 2 SAMPLES. 69
TABLE 11. ZETA POTENTIAL MEASUREMENTS OF GAN (TOPO) BEFORE AND AFTER SOLUBILIZING WITH PHOSPHOLIPIDS CONTAINING CARBOXYL TERMINI. 71
TABLE B 1. POLAND AND SOVIET UNION STUDIES IN HUMAN PHAGE THERAPY. (76)....78

LIST OF FIGURES

FIGURE 1. M13 BACTERIOPHAGE STRUCTURE. (IMAGE COURTESY OF AHMAD KHALIL, BELCHER LAB) 11
FIGURE 2. M13 BACTERIOPHAGE GENOME. NEW ENGLAND BIOLABS 12
FIGURE 3. M13 BACTERIOPHAGE REPLICATION CYCLE. (PICTURE COURTESY OF HTTP://WINE1.SB.FSU.EDU/BCH5425/LECT33/LECT33.HTM) 13
FIGURE 4. BIOPANNING SCHEMATIC THROUGH ONE ROUND OF SELECTION. PHAGE IS INTERACTED WITH A GIVEN MATERIAL AND NONSPECIFIC PHAGE ARE WASHED OFF. TIGHTLY BINDING PHAGE THEN ARE ELUTED VIA PH ELUTION OR ANTIBODY ELUTION AND COLLECTED AND AMPLIFIED FOR THE NEXT ROUND OF SELECTION. (26). 15
FIGURE 5. LIST OF VACCINES KEPT AT 2-8°C. (29) 17
FIGURE 6. LIQUID CRYSTAL PHASES OF PHAGE. (A) NEMATIC, (B) SMECTIC A, AND (C) SMECTIC C PHASE, WHERE THE AXIS IS TILTED. (34) 20
FIGURE 7. CHIRAL SMECTIC C M13 VIRUS FILMS. (A) PHOTOGRAPH OF THE M13 VIRUS FILM. (B) SCHEMATIC DIAGRAM OF THE M13 VIRUS FILM STRUCTURE IN BULK WHICH HAS A CHIRAL SMECTIC C ORDERING STRUCTURE (Z, DIRECTOR; N, LAYER NORMAL; Θ, TILT ANGLE; Φ, AZIMUTHAL ROTATION ANGLE). (C) SCHEMATIC DIAGRAM OF THE SURFACE MORPHOLOGY OF THE M13 VIRUS FILM FOR WHICH THE HELICAL ORDERING STRUCTURE IS UNWOUND AND FORMED A ZIGZAG PATTERN DUE TO SURFACE EFFECTS. (D) POLARIZED OPTICAL MICROSCOPY IMAGE OF VIRAL FILM AT 9.93 MG/ML SHOWING THE DARK AND BRIGHT STRIPE PATTERNS (SCALE BAR 100μM). (E) LASER LIGHT DIFFRACTION PATTERN FROM VIRAL FILM. (14) REPRINTED WITH PERMISSION FROM (14). COPYRIGHT (2003) AMERICAN CHEMICAL SOCIETY. 20
FIGURE 8. SCHEMATIC OF ORDERING PROTEIN-BASED VACCINE IN M13 VIRUS FILM. THE M13 BACTERIOPHAGE (BLUE) IS SELECTED VIA THE P3 AGAINST THE PROTEIN OF INTEREST (RED) AND COMBINED TOGETHER, SELF-ASSEMBLES INTO A HYBRID SELF-SUPPORTING FILM. 21
FIGURE 9. FIREFLY LUCIFERASE RIBBON STRUCTURE. THE LARGE N-TERMINAL DOMAIN (AMINO ACIDS 1-436) IS CONNECTED TO THE SMALLER C-TERMINAL DOMAIN (AMINO ACIDS 440-550 SHOWN IN YELLOW) THROUGH A SHORT HINGE PEPTIDE (35, 36) 22
FIGURE 10. LUCIFERASE BIOLUMINESCENCE REACTION. MONO-OXYGENATION OF LUCIFERIN CATALYZED BY LUCIFERASE IN THE PRESCENCE OF Mg^{2+}, ADENOSINE TRI-PHOSPHATE (ATP), AND OXYGEN. (COURTESY OF PROMEGA CORP.) 22
FIGURE 11. DETAILED MECHANISM OF FIREFLY BIOLUMINESCENCE AND VARIATIONS IN COLOR. * INDICATES AN ELECTRONIC EXCITED STATE (35). 23
FIGURE 12. SCHEMATIC OF LUCIFERASE INTERACTION WITH LUCIFERIN. THE DOTTED LINES INDICATE HYDROGEN BONDING BETWEEN LUCIFERASE AND SUBSTRATES LUCIFERIN (GREEN), ATP (VIOLET), AND Mg^{2+} PREDICTED BY MOLECULAR MODELING. THE CURVED BLUE ARROWS REPRESENT THE NUCLEOPHILIC ATTACK OF THE LUCIFERIN CARBOXYLATE AT THE A-PHOSPHORUS OF ATP AND THE CORRESPONDING FORMATION OF THE PENTAVALENT INTERMEDIATE (35) 24
FIGURE 13. BIOPANNING ROUND 3 PHAGE ELUATE PEPTIDE SEQUENCING RESULTS. THE LETTERS REPRESENT AMINO ACIDS AND THE COLORS GROUP THEM INTO CATEGORIES BASED ON THEIR R GROUPS: ACIDIC (RED), BASIC (BLUE), HYDROPHOBIC (ORANGE), HYDROXYL (GREEN), RING GROUPS (TAN), PROLINE (YELLOW), AMIDE (PURPLE), AND METHIONINE (WHITE). THE SEQUENCES HAVE BEEN ORDERED IN SUCH A WAY TO HIGHLIGHT THE DOMINANT SEQUENCE WITH TWELVE OCCURRENCES OUT OF A TOTAL OF 20 SEQUENCES: CKLHGTSRC. ANOTHER SEQUENCE THAT WILL OCCUR IN A SUBSEQUENT EXPERIMENT OF NOTE IS CTKRNNKRC. 29
FIGURE 14. ELISA RESULTS FOR CLONE PL3 AND CONTROLS. M13KE IS THE WILD-TYPE M13 PHAGE AND P3S1 IS THE STREPTAVIDIN-BINDING PHAGE. 31
FIGURE 15. ABSORBANCE VS EXPECTED PHAGE CONCENTRATION FROM ELISA. M13KE IS THE WILD-TYPE M13 PHAGE AND P3S1 IS THE STREPTAVIDIN-BINDING PHAGE. THE READINGS WERE NORMALIZED WITH A BLANK SUBTRACTION 32
FIGURE 16. BIOPAN ROUND 4B DNA SEQUENCING RESULTS, REORDERED. THE LETTERS REPRESENT AMINO ACIDS AND THE COLORS GROUP THEM INTO CATEGORIES BASED ON THEIR R GROUPS: ACIDIC (RED), BASIC (BLUE), HYDROPHOBIC (ORANGE), HYDROXYL (GREEN), RING GROUPS (TAN), PROLINE (YELLOW), AMIDE (PURPLE), AND METHIONINE (WHITE) 33
FIGURE 17. ELISA WELL SCHEMATIC AND RESULTS FOR AMPLIFIED CLONES 1-5. THE DILUTION FACTORS ON THE BOTTOM ARE WITH RESPECT TO THE PREVIOUS WELL AND ND REPRESENTS NO DILUTION. 35
FIGURE 18. LUCIFERASE ELISA WITH CLONES 1-5 AND M13KE CONTROL. 36

FIGURE 19. LUCIFERASE ELISA OF CLONES 1-5 WITH M13KE CONTROL. THIS GRAPH IS FOCUSED ON THE EXPONENTIAL GROWTH PHASE OF THE CURVES FROM FIGURE 18. 36
FIGURE 20. M13 VIRUS FILM WITH LUCIFERASE. SEM IMAGE (JEOL 6320 FV) 40
FIGURE 21. VENOUS LEG ULCER FROM MULTI-DRUG RESISTANT BACTERIAL INFECTION SUCCESSFULLY TREATED WITH PHAGE. PICTURES REPRODUCED, WITH PERMISSION, COURTESY OF DR. RANDALL WOLCOTT, SOUTHWEST REGIONAL WOUND CARE CENTER, TEXAS. (45) 45
FIGURE 22. VIRUS BASED PLATFORM FOR DETECTING CANCER. THE CANCER CELL RECEPTOR IS MERELY A RECEPTOR OR PROTEIN THAT IS UPREGULATED IN PARTICULAR TYPES OF CANCERS AND HAS BEEN ESTABLISHED AS A MARKER FOR THAT TYPE OF CANCER – FOR EXAMPLE, THE VCAM-1 RECEPTOR FOR BREAST CARCINOMA. THE CANCER TARGETING PEPTIDE (CTP) CAN ALSO BE INTERCHANGED WITH THE NANOPARTICLE SO THAT THE CTP IS ON THE P3 AND NANOPARTICLE IS ON THE P8. 50
FIGURE 23. POLYACRYLAMIDE GEL (2-40% TBE POLYACRYLAMIDE GEL) PURIFICATION OF RANDOM OLIGONUCLEOTIDE INSERT AND M13SK VECTOR IN PREPARATION FOR LIGATION. THE ARROWS INDICATES BANDS OF INTEREST. AND NUMBERS TO THE LEFT OF THE GELS ARE IN UNITS OF BASE PAIRS. (A) DIGESTED INSERT GEL (B) AFTER REMOVING DIGESTED INSERT BAND (C) VECTOR, WHERE THE LAST COLUMN IS THE UNDIGESTED VECTOR WHICH STILL RETAINS THE CIRCULAR RF FORM (D) AFTER REMOVING DIGESTED VECTOR BAND. 52
FIGURE 24. SCHEMATIC FOR CONSTRUCTION OF TYPE 8 PHAGE LIBRARY IN M13SK. SCHEMATIC SHOWS THE RESTRICTION SITES FOR CLONING DNA LIBRARY INTO M13SK. X = ANY RANDOMIZED AMINO ACIDS. (34) 53
FIGURE 25. TYPE 83 GENETIC ENGINEERING OF M13 BACTERIOPHAGE. SEE ALSO APPENDIX C 54
FIGURE 26. P8#9 AND P8E4 TYPE 8 BACTERIOPHAGE COMBINED WITH VCAM1-LINEAR AND VCAM1-CYCLIC SEQUENCES ON PIII 55
FIGURE 27. P8E4 MUTATION. SPONTANEOUS MUTATION OF P8E4 PHAGE TO P8E3 PHAGE THROUGH DELETION OF ONE GLUTAMATE 55
FIGURE 28. QUANTUM DOT CHARACTERISTICS. (A) RELATIVE SIZES AND EMISSION WAVELENGTHS OF VARIOUS QUANTUM DOTS (95) (B) GRAPH COMPARING THE PHOTO-BLEACHING OF QUANTUM DOTS AND ORGANIC DYES (96) (C) FLUORESCENCE INDUCED BY EXPOSURE TO ULTRAVIOLET LIGHT IN VIALS CONTAINING VARIOUS SIZED CADMIUM SELENIDE (CDSE) QUANTUM DOTS. (COURTESY OF DR. D. TALAPIN, UNIVERSITY OF HAMBURG, HTTP://WWW.CHEMIE.UNI-HAMBURG.DE/PC/WELLER/). 59
FIGURE 29. USES OF QUANTUM DOTS IN BIOLOGICAL IMAGING. 60
FIGURE 30. E3S1 M13 BACTERIOPHAGE ON SILICON WAFER. 63
FIGURE 31. E3S1 M13 BACTERIOPHAGE COATED WITH AMINE-TERMINATED CDSE/ZNS QUANTUM DOTS. Q 63
FIGURE 32. 4-NM ZNS COATED CDSE QDOTS IN PHOSPHOLIPID BLOCK CO-POLYMER MICELLE. REPRINTED WITH PERMISSION FROM (106). COPYRIGHT (2002) AAAS. 64
FIGURE 33. NHS-MALEIMIDE FUNCTIONALIZING OF QUANTUM DOTS 65
FIGURE 34. AMPHIPHILIC POLYMERS USED TO WATER SOLUBILIZE GAN AND INN QUANTUM DOTS 67
FIGURE 35. SCHEMATIC FOR WATER SOLUBILIZING GAN AND INN QUANTUM DOTS. 68
FIGURE 36. GAN OR INN QUANTUM DOTS SURROUNDED BY PHOSPHOLIPIDS. 70
FIGURE 37. WATER SOLUBILIZED GAN (CTAB). 71
FIGURE 38. WATER SOLUBLE INN QUANTUM DOTS 72
FIGURE 39. TEM WITH EDX ANALYSIS OF WATER SOLUBILIZED INN. 73
FIGURE A1. BIOPANNING ROUND 2 ELUTED PEPTIDE SEQUENCES. THE LETTERS REPRESENT AMINO ACIDS AND THE COLORS GROUP THEM INTO CATEGORIES BASED ON THEIR R GROUPS: ACIDIC (RED), BASIC (BLUE), HYDROPHOBIC (ORANGE), HYDROXYL (GREEN), RING GROUPS (TAN), PROLINE (YELLOW), AMIDE (PURPLE), AND METHIONINE (WHITE) 76
FIGURE A2. BIOPANNING ROUND 2B ELUTED PEPTIDE SEQUENCES. THE LETTERS REPRESENT AMINO ACIDS AND THE COLORS GROUP THEM INTO CATEGORIES BASED ON THEIR R GROUPS: ACIDIC (RED), BASIC (BLUE), HYDROPHOBIC (ORANGE), HYDROXYL (GREEN), RING GROUPS (TAN), PROLINE (YELLOW), AMIDE (PURPLE), AND METHIONINE (WHITE) 76
FIGURE A3. BIOPANNING ROUND 3B ELUTED PEPTIDE SEQUENCES. THE LETTERS REPRESENT AMINO ACIDS AND THE COLORS GROUP THEM INTO CATEGORIES BASED ON THEIR R GROUPS: ACIDIC (RED), BASIC (BLUE), HYDROPHOBIC (ORANGE), HYDROXYL (GREEN), RING GROUPS (TAN), PROLINE (YELLOW), AMIDE (PURPLE), AND METHIONINE (WHITE) 77
FIGURE C1. OVERLAP EXTENSION PCR FOR PVIII CLONING SITES 81

CHAPTER 1 – Introduction

1.1 Thesis Overview

The versatile nature of the M13 bacteriophage lends itself to a myriad of applications in biomedical engineering. In this thesis, I will present two examples of how phage can be manipulated and incorporated in some of the most cutting-edge biomedical research today. The thesis will have two parts, one on the use of phage for heat-stable vaccine storage and the other on the creation of a virus-based multifunctional platform for *in vivo* cancer diagnostics.

1.2 Phage Biology

Bacteriophage or phage, are viruses that infect only bacteria. They were first described in 1915 by Frederick Twort and 1917 by Felix d'Herelle. Both scientists discovered phage when the bacteria they were working with lysed. The entity responsible for the lysis was transferable from culture to culture and was able to bypass the smallest filters they had. D'Herelle called them "bacteriophage", representing something that eats bacteria.

Comprised of only a nucleic acid molecule surrounded by a protective capsid, phage are simple. There are many types of phage. They differ in their nucleic material and replication behavior. Some lyse their host bacteria while others do not. The process of infecting the bacterial host and producing progeny along with lysis of the host is called lytic infection. T4 phage is only capable of lytic growth, while P1 and λ are capable of both lytic and lysogenic behavior. Lysogeny is the process where the phage maintains its chromosome in a stable, silent state within the bacteria, integrating into the host genome. When host conditions deteriorate, the lytic machinery becomes active again and the phage exits the host, killing it. (1)

However, some phage can enter, replicate, and exit their hosts without killing them (chronic or continuous infecting phage). (2) The filamentous phage (e.g., M13, fd, or f1) are as such and do not kill their *E.coli* hosts but develop a symbiotic relationship in which new virions are continually released by a secretory mechanism. (3)

The M13 bacteriophage is of the filamentous phage family (due to its anisotropic shape) and contains a circular single-stranded DNA genome with 6,407 nucleotides surrounded by five proteins. On one end, there are five copies each the minor p3 protein (60-65 kDa) and approximately 5 copies of the p6 protein. On the other end are three copies of p9 and four copies of p7. Along the entire length of the phage, there are 2,700 copies of the major p8 coat protein (Figure 1).(4)

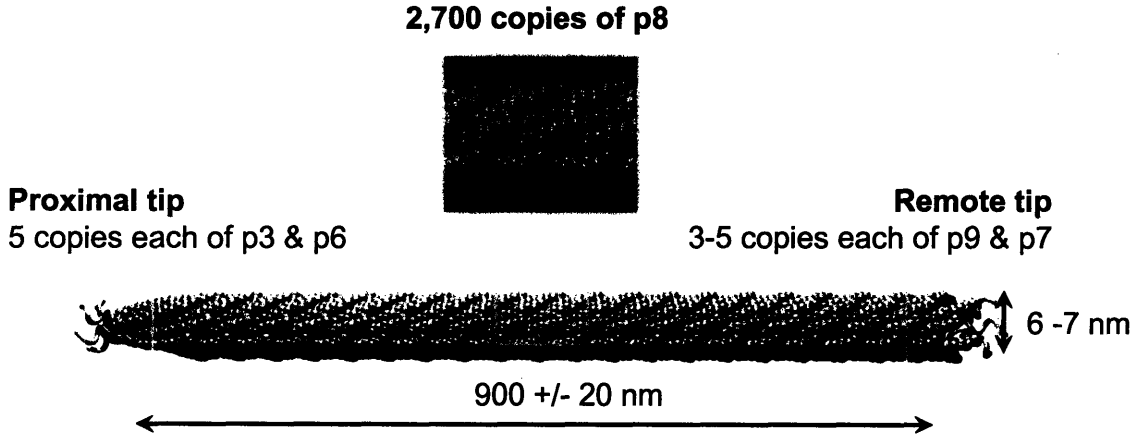

Figure 1. M13 Bacteriophage Structure. (Image courtesy of Ahmad Khalil, Belcher Lab)

The M13 Genome is shown in Figure 2. The regions before gIII and gVIII can be engineered to express different peptides on the p3 and p8 coat proteins. The region between gII and gIV is also

often used as the site for inserting foreign DNA, and this region contains the Multiple Cloning Site (MCS).

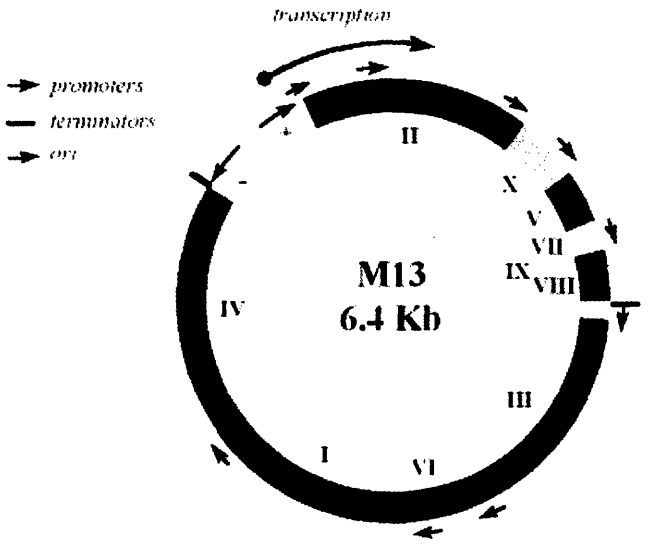

Figure 2. M13 Bacteriophage Genome. New England Biolabs

The phage infection and reproduction cycle is rapid. Phage transcripts are detected after 2 minutes (3, 5, 6), and the major phage mRNAs are generated sequentially over a 10 minute period after infection (3, 5). The first release of phage progeny occurs 15-20 minutes after infection (3, 5, 7).

Replication is initiated when the M13 bacteriophage p3 protein adsorbs to the tip of the F pilus on the surface of *E.coli*. The p3 then interacts with the inner membrane protein TolA and forms a pore large enough for DNA to go through. The circular single-stranded M13 DNA is released into the cytoplasm of the bacterial host and this (+) strand is immediately coated with the *E.coli* single-stranded DNA binding protein, SSB. SSB protects the DNA from degradation. The M13

(+) strand is converted to a double-stranded molecule immediately, and the synthesis of the complementary (-) strand is done by the *E.coli* DNA synthesis machinery. The SSB that binds to the (+) strand fails to bind to ~ 60 nucleotides of the DNA and this section forms a hairpin loop, which is found to be associated with the M13 p3. This hairpin loop is recognized by the *E.coli* RNA polymerase as a DNA replication origin and is used to initiate transcription of a short RNA primer. The RNA primer is extended by *E.coli* DNA polymerase III to form the (–) strand while the primer is later removed by *E.coli* DNA polymerase I with its exonuclease activity. *E.coli* ligase helps form the final closed double-stranded circular M13 chromosome called the replicative form (RF) DNA. The RF form replicates by rolling circle replication (Figure 3), and while the chromosome is being replicated, the genes encoding the coat proteins are being transcribed and translated.

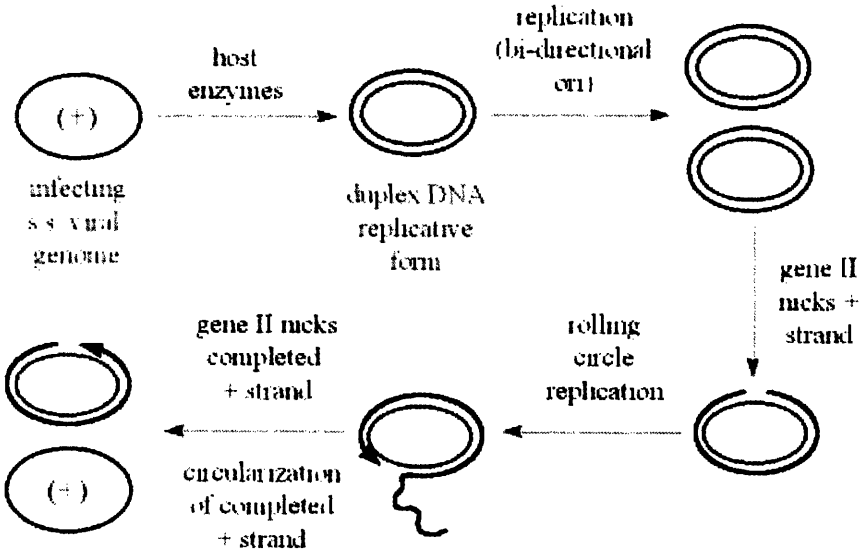

Figure 3. M13 Bacteriophage Replication Cycle. (Picture courtesy of http://wine1.sb.fsu.edu/bch5425/lect33/lect33.htm)

When another M13 protein, p5, accumulates to sufficient levels, a switch from synthesizing RF DNA to synthesizing the (+) strand occurs. Gene V blocks the synthesis of the (–) strand, and as

a result, the (+) strand is circularized. The M13 phage particles are assembled through a non-lytic process. The p5 coated (+) strand interacts with the bacterial inner membrane, which requires specific packaging sequences on the DNA and p7 and p9. The protein-coated DNA passes through the membrane and along the way, p5 is replaced by p8. When the last of the phage particle crosses the membrane, p2 and p6 are added, and it has been shown that p6 is responsible for termination of phage assembly (1, 3, 8). Up to 1000 phage particles are released into the medium per cell per generation of replication (9).

Although M13 phage does not cause bacterial death, it does have some effect on its host. The *E.coli* grows more slowly, creating plaques on agar plates (ie. zone of slower growth and lower density of bacteria) and also becomes more acid sensitive (3) due to down regulation in transcription of acid resistance genes. For the most part, however, the effect is minor.

1.3 Phage Display

Phage display is a process whereby small sequences of peptides are expressed on the coat proteins of phage, forming a phage display library. Phage libraries are large populations of phage that have expressed, on either its p3 or p8, a wide range of different peptides of the same length but different sequences. These libraries can be used to screen against various organic or inorganic materials in a selection process for identifying the peptides with highest affinity for that material. The peptide sequences, with or without the phage, can then be used in devices, phage-material films, or a number of self-assembly applications. (10-20) In general, the process of phage screening or biopanning starts with a library of phage. This library is interacted with the target material. Some of the phage will bind, while non-binders or weakly bound phage are

removed through a series of washing steps. Only the strongest binding phage will remain on the surface. The tight binding phage are then eluted from the surface using either a pH elution, temperature, competitive binding, or antibody elution. The eluate is then amplified up again in bacteria (e.g. *E.coli*) and used for the next round of biopanning, replacing the library as the interaction species. Using this process, multiple rounds of screening are done, and after each round, the DNA sequences of the phage are translated into peptide sequences. The peptide sequences are checked to see if there is any consensus among the sequences (ie. multiple occurrences of the same sequence), which would indicate a dominant binder. For organic materials, we can usually see a consensus sequence by the 3rd or 4th round, but for inorganic materials, often 5 rounds are needed. Figure 4 shows the general schematic for biopanning. The materials that phage can be used to select against are very diverse, ranging from enzymes to cell surface receptors, semiconductors, and quantum dots (11, 16, 21-25).

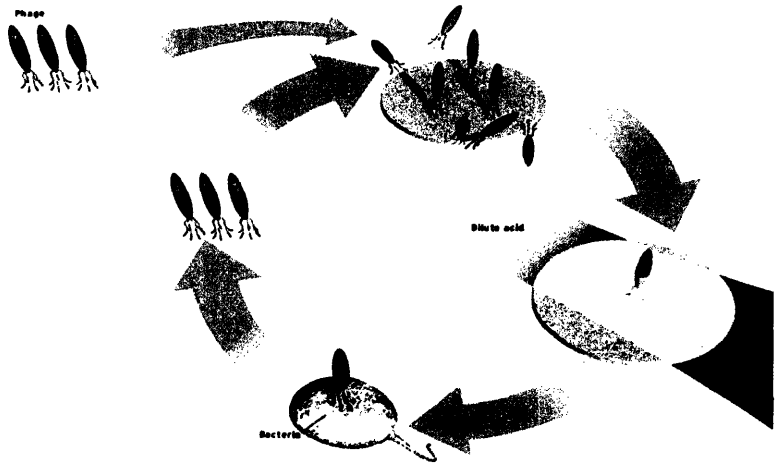

Figure 4. Biopanning Schematic Through One Round of Selection. Phage is interacted with a given material and nonspecific phage are washed off. Tightly binding phage then are eluted via pH elution or antibody elution and collected and amplified for the next round of selection. (26)

CHAPTER 2 – Vaccine Storage System Based On The M13 Bacteriophage

2.1 Abstract

Conventional vaccine storage forms require refrigeration or freezing, leading to high cost and difficult field delivery. Thermal degradation results in the non-viability of a substantial fraction of drugs delivered. By capitalizing on the liquid crystalline nature and unique diffraction patterns of phage film systems, we are working to encapsulate vaccines in a 3-D liquid crystalline matrix that would not only allow for stability at elevated temperatures, but would also allow easy detection of viability by simply shining a laser at the virus film and noting the changes in diffraction pattern. The release of vaccine would follow from dissolution of the storage system, ideally in a sustained release manner.

2.2 Introduction

2.2.1 Vaccine Storage and Protein-Based Vaccines

The problem of vaccine storage, especially in field conditions in developing countries where vaccines are most needed, rests in the cold chain. The cold chain system is the process of transporting and storing vaccines within the safe temperatures of 2-8°C from the place of manufacture to the point of administration. A break in the cold chain results in either an inactivated vaccine or reduced shelf life. For example, the measles vaccine, even while lyophilized, loses potency at high temperatures, with a half life of 31 days, 16.6 days, or 3.3 days at temperatures of 25-30°C, 37, or 41°C, respectively (27). Other vaccines like the varicella

vaccine and live attenuated influenza vaccine (LAIV) must be stored at below -15°C, and any increase in temperature can inactivate the vaccine (28). Figure 5 shows a list of vaccines and testing solutions that must be stored between 2-8°C (29).

Vaccines that must be stored between 2-8°C

- Diphtheria and tetanus toxoids
- Diphtheria and tetanus toxoids, and pertussis vaccine (acellular)
- Diphtheria and tetanus toxoids, pertussis vaccine (acellular), inactivated polio vaccine and Haemophilus influenzae type b (Hib) conjugate vaccine
- Hepatitis A vaccine
- Hepatitis B vaccine
- Hib conjugate vaccine
- Inactivated polio vaccine
- Influenza vaccine
- Measles, mumps, and rubella vaccine
- Meningococcal C vaccine
- Pneumococcal 7-valent conjugate vaccine
- Pneumococcal polysaccharide 23-valent vaccine
- Rabies vaccine
- Rabies immune globulin
- Tuberculosis testing solution
- Varicella vaccine

Figure 5. List of Vaccines Kept at 2-8°C. (29)

Vaccines need to be stored at low temperatures in order to prevent thermal degradation from denaturation of tertiary structure of the proteins that make up the vaccines or that are part of the microorganisms forming the vaccine. However, not only does the need for refrigeration of a vaccine cost money in terms of electricity, but it's just purely not feasible in some remote parts of underdeveloped countries that do not have access to electricity. In addition, because the range of temperatures for maintaining viability in these vaccines is very narrow, any deviation from that range will cause impotency, which is a difficult measurement to make in the field, requiring sophisticated laboratory equipment such as spectrophotometers, and fluorimeters. As a result, much of the vaccine that is actually being administered is no longer viable, putting the patient at risk. If we can develop a vaccine storage technology that will allow room temperature or

elevated temperature (up to 40°C) storage of vaccines, more of the developing world can be reached, lives can be saved, and cost can be cut.

Conventional vaccines include live-attenuated microbes, inactivated microorganisms, purified microbial components, polysaccharide-carrier protein conjugates, and recombinant proteins. The diphtheria and tetanus toxoids vaccine is an example of a protein-based vaccine and was developed in the first half of the twentieth century (30). Vaccines based on protein antigens have considerable promise because of their low toxicity and widespread applicability and constitute a new vaccination strategy that is increasingly being investigated for the new generation of vaccines (31). Protein-based vaccines tend to induce more of a humoral immune response rather than a cellular one, so would naturally be more effective against extracellular pathogens (30). Protein-based vaccines are also more amenable for encapsulation within a phage based film due to its smaller size (as compared to microorganisms) and therefore will be used as our first vaccine storage candidate.

2.2.2 M13 Bacteriophage as a Liquid Crystal

Liquid crystals have an ordered state in between that of solids and liquids. For example crystalline materials exhibit long range periodic order in three dimensions while isotropic liquid has no orientational order. Liquid crystals are not as ordered as solids but have some degree of alignment. The distinguishing characteristic of the liquid crystalline state is the tendency of the molecules to point along a common axis. There are three main types of liquid crystal phases: nematic, smectic, and cholesteric.

The nematic phase is characterized by molecules that have no positional order but tend to point in the same direction. The smectic phase is more ordered and shows a degree of translational order not seen in the nematic phase. The molecules maintain the general orientation of the nematics but also tend to align themselves in layers or planes. Motion is restricted to within these planes and the separate planes are observed to flow past each other. Within the smectic classification, there are a several subclasses. In the smectic A mesophase, the director is perpendicular to the smectic plane, and there is no particular positional order in the layer. The smectic B mesophase orients with the director perpendicular to the smectic plane, but the molecules are arranged into a network of hexagons within the layer. In the smectic C mesophase, the molecules are arranged as in the smectic A mesophase, but the director is at a constant tilt angle with respect to the smectic plane. The smectic C mesophase has also a chiral counterpart where the tilt angle changes from layer to layer as to form a helix. The last class is the cholesteric phase, which is like the nematic but contains a chiral center, which causes alignment between molecules at a slight angle to each other. A defining characteristic of the cholesteric phase is the pitch, which is the distance it takes for the director to rotate one full turn in the helix. Due to this property, one can selectively reflect light of wavelengths equal to the pitch length, so that a color will be reflected when the pitch is equal to the corresponding wavelength of light in the visible spectrum.

It has been shown that several types of rod-shaped viruses form well-controlled liquid-crystalline phases (13, 32, 33). Phage can form nematic, smectic A, or smectic C phases as shown in Figure 6 and in our laboratory, we have shown that M13 bacteriophage can be fabricated into films that exhibit smectic A, C, or chiral smectic C structures (14). (Figure 7) Higher concentrations of phage are required for forming smectic phase films than nematic phase films.

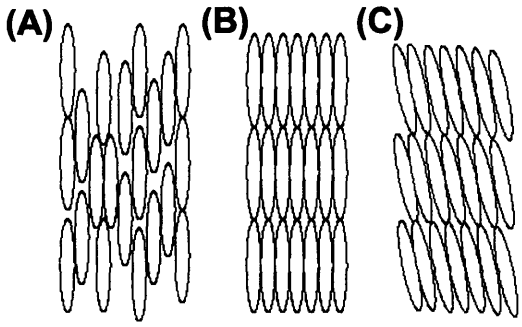

Figure 6. Liquid Crystal Phases of Phage. **(A)** Nematic, **(B)** Smectic A, and **(C)** Smectic C phase, where the axis is tilted. (34)

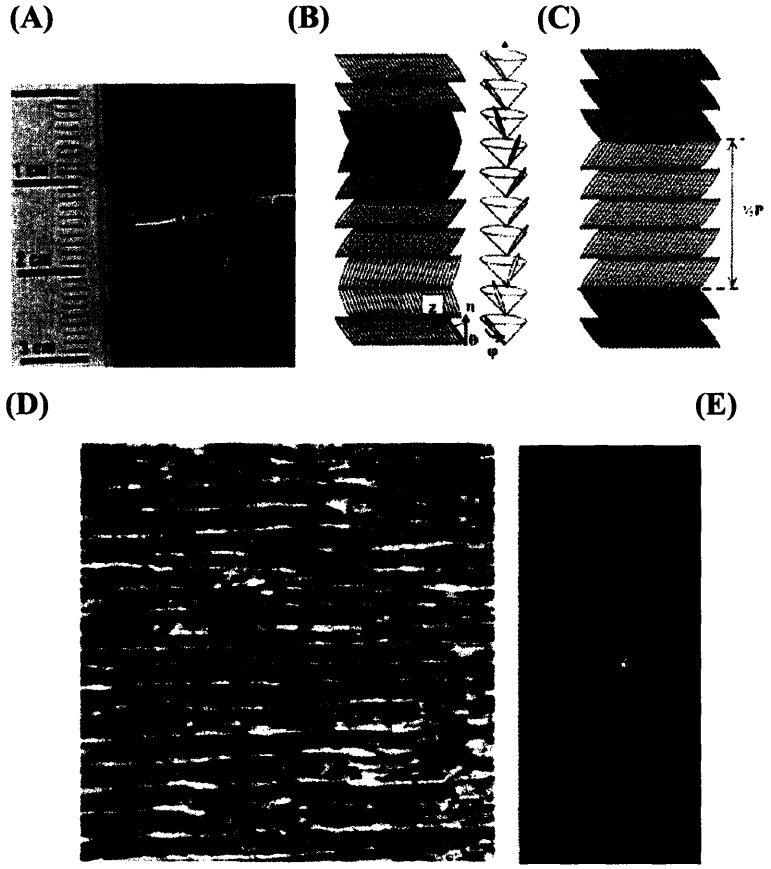

Figure 7. Chiral Smectic C M13 Virus Films. **(A)** Photograph of the M13 virus film. **(B)** Schematic diagram of the M13 virus film structure in bulk which has a chiral smectic C ordering structure (z, director; n, layer normal; θ, tilt angle; φ, azimuthal rotation angle). **(C)** Schematic diagram of the surface morphology of the m13 virus film for which the helical ordering structure is unwound and formed a zigzag pattern due to surface effects. **(D)** Polarized optical microscopy image of viral film at 9.93 mg/ml showing the dark and bright stripe patterns (scale bar 100μm). **(E)** Laser light diffraction pattern from viral film. (14) Reprinted with permission from (14). Copyright (2003) American Chemical Society.

2.2.4 Stabilizing Vaccines within Liquid Crystalline Phage Films

The idea for using a phage film for storage of vaccines is based on the concept of structural stability. The combination of the ability of the M13 bacteriophage to be genetically manipulated as well as the ability to form liquid crystal films gives it the capability to bind specifically to a protein-based vaccine and confine it three-dimensionally in a phage film. The hypothesis is that this three-dimensional confinement would maintain structural integrity and biological viability of the vaccine. The rational is that if the protein-based vaccine can be kept in its native conformational state by virtue of being trapped within the aligned phage film, its activity can be preserved. The self-assembling M13 virus building blocks can be combined, using phage selection, with the protein vaccine of interest to form hybrid self-supporting films that can serve as storage units for the vaccines. Figure 8 shows the general schematic of one layer of the phage-protein film.

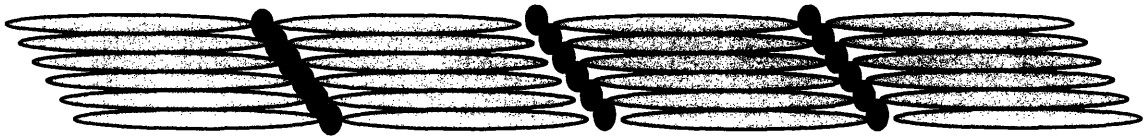

Figure 8. Schematic of Ordering Protein-Based Vaccine in M13 Virus Film. The M13 bacteriophage (blue) is selected via the p3 against the protein of interest (red) and combined together, self-assembles into a hybrid self-supporting film.

Figure 7E shows the diffraction pattern visible upon shining a laser light on a phage film. This analytical technique can be used in the field in developing countries to check on the structural integrity of the virus film and therefore, is an inexpensive and easy way of verifying stability of the vaccine.

2.2.3 Luciferase

As an initial *in vitro* model for our protein-based vaccine, we identified a protein with readily determined reporter characteristics and also reasonable thermal instability to mimic the instability of potential vaccine candidates. We chose the bioluminescent enzyme Firefly Luciferase. The three-dimensional structure of Firefly Luciferase is shown in Figure 9 (35).

Figure 9. Firefly Luciferase Ribbon Structure. The large N-terminal domain (amino acids 1-436) is connected to the smaller C-terminal domain (amino acids 440-550 shown in yellow) through a short hinge peptide (35, 36).

Bioluminescence is a process in which living organisms convert chemical energy into light. Firefly Luciferase is a 61kDa monomer that catalyzes the mono-oxygenation of beetle luciferin (Figure 10).

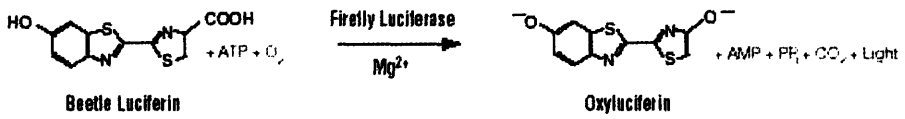

Figure 10. Luciferase Bioluminescence Reaction. Mono-oxygenation of luciferin catalyzed by luciferase in the prescence of Mg^{2+}, adenosine tri-phosphate (ATP), and oxygen. (Courtesy of Promega Corp.)

Beetle luciferin is a molecule found in beetles, including fireflies, and the reaction in Figure 10 is what causes fireflies to light up at night. Luciferase gets most of its energy for photon generation

from oxygen but also uses adenosine tri-phosphate (ATP) as a cofactor. The quantum yield is 0.9, the highest of any known luminescent reaction.

The generally accepted mechanism of firefly bioluminescence is presented in Figure 11 (35).

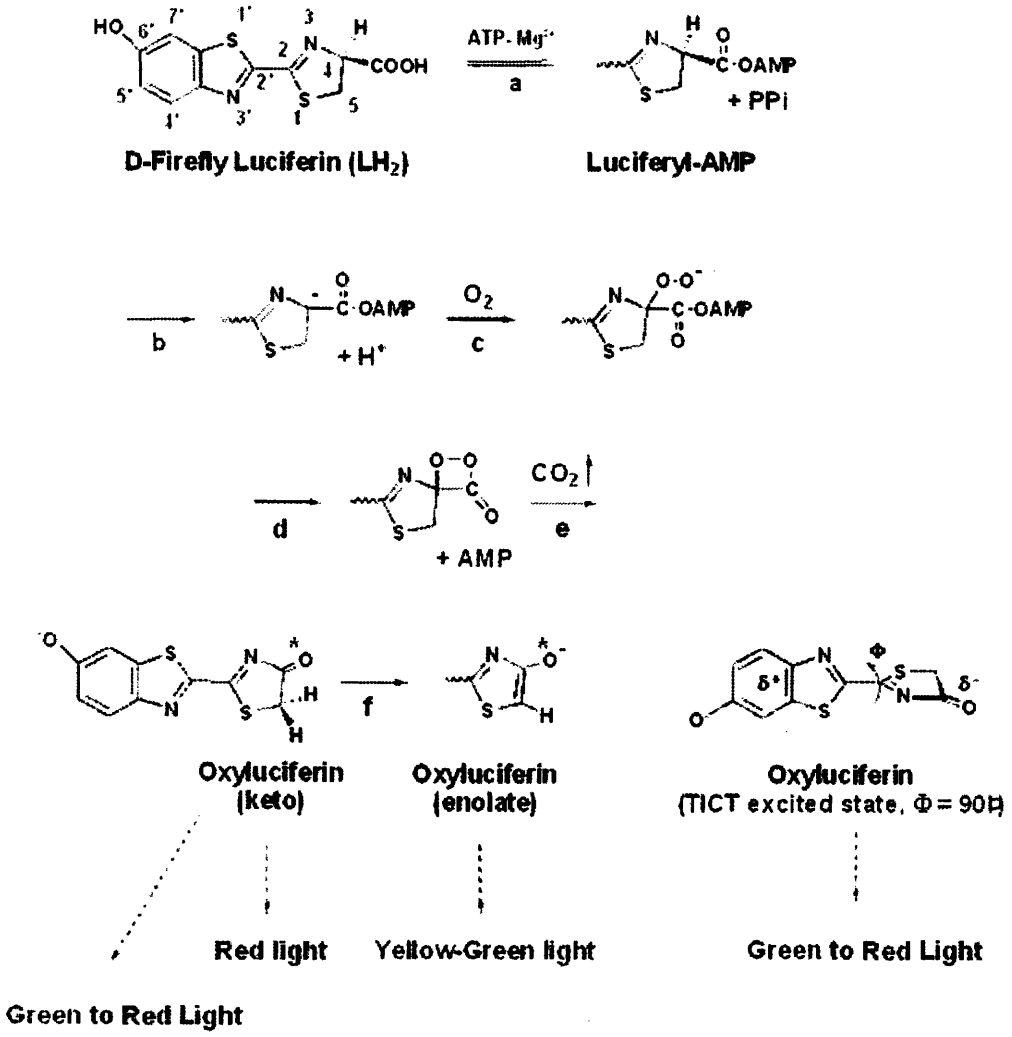

Figure 11. Detailed Mechanism of Firefly Bioluminescence and Variations in Color. * Indicates an electronic excited state (35).

Structurally, it has been determined how luciferase binds to its substrate and cofactors and this schematic is shown in Figure 12.

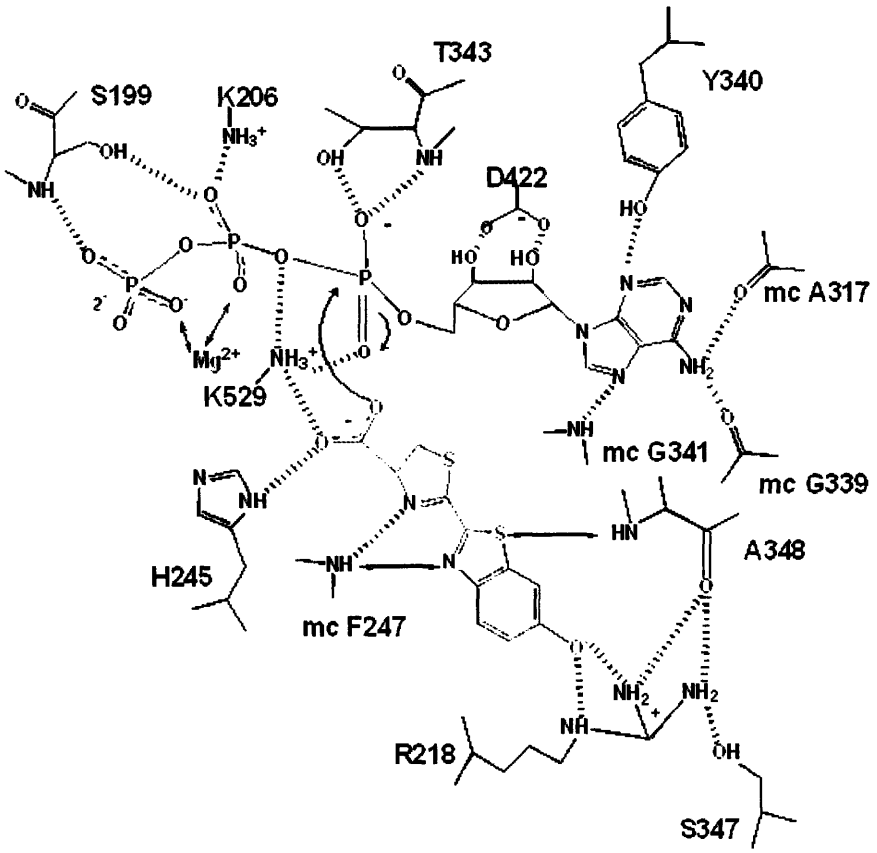

Figure 12. Schematic of Luciferase Interaction with Luciferin. The dotted lines indicate hydrogen bonding between luciferase and substrates luciferin (green), ATP (violet), and Mg^{2+} predicted by molecular modeling. The curved blue arrows represent the nucleophilic attack of the luciferin carboxylate at the α-phosphorus of ATP and the corresponding formation of the pentavalent intermediate (35).

The active site of luciferase is shown in Figure 12, encircling the substrate luciferin (green). Some of the motifs important for binding to luciferin are R218 (Arginine, position 218), which maintains the rigidity of the protein to emit light, and a β-hairpin motif that interacts with the active site (^{442}IleLysTyrLysGlyTyrGlnVal^{449}). 443Lys promotes the first step of the reaction (LH_2-AMP formation), and Lys529 promotes the oxidation to produce light. In addition, R218, F247, A348, H245, and K529 fix the position of luciferin in the binding pocket (37). These active site motifs will be compared to sequences selected through experimentation to ensure that the sequences do not inhibit activity.

2.3 Methods, Results, and Discussion

2.3.1 Overview

The experimental plan for determining protein-stabilization properties of phage films was divided into three stages. The first stage involved phage selection (ie. biopanning) to identify the peptide-expressing M13 bacteriophage that had an affinity to luciferase and therefore interacted with luciferase in such a way as to encase it in a liquid crystalline structure. Second, the affinity of the selected peptides was validated using Enzyme-Linked ImmunoSorbant Assay (ELISA). The final step was assembly of the luciferase and liquid crystalline films, while monitoring the stability of the encapsulated luciferase.

2.3.2 Luciferase

Firefly luciferase was purchased from Sigma (St. Louis, MO) and was reconstituted in 50 mM Tris-HCl pH 8.0, 1 mM dithiothreitol, 1 mM EDTA, and 10% (v/v) glycerol to form a stock concentration of 430.60 µg/ml, which was then aliquoted into 50 µl aliquots in 1.5ml eppendorfs and stored at -80°C.

2.3.3 Biopanning

Methods

Four rounds of biopanning against luciferase were conducted. In each round, the target substrate was prepared as 200 µl of 100 µg/ml luciferase in 0.1 M $NaHCO_3$ pH 8.6 and pipetted into one well of a polystyrene 24 well plate. The luciferase was allowed to coat the plate overnight in a 4°C humidified chamber. A chamber was created simply from a Tupperware container large

enough to hold the well plate and then lined with wet paper towels. The next day, excess luciferase solution was withdrawn carefully with a pipet, and the target well was blocked for 1 hour at 4°C in a humidified chamber with 1.5 ml of blocking buffer (0.1 M $NaHCO_3$ pH 8.6, 5mg/ml BSA). The solution was then withdrawn and the well was washed six times with TBST 0.1% (50mM Tris-HCl pH 7.5, 150mM NaCl, 0.1% Tween-20). After the last wash, M13 bacteriophage 7-mer constrained p3 library (Ph.D.^{TM}-C7C Phage Display Peptide Library, New England Biolabs) was interacted with the target as a 200 µl solution (in TBST 0.1%) at a twenty fold dilution of the library: $1x10^9$ pfu/µl. The bacteriophage library was allowed to interact for 1 hour at room temperature on a shaker, after which the well was washed ten times with TBST 0.1%. The phage that remained on the luciferase target was then pH eluted with 0.1 ml of 0.2M Glycine-HCl pH 2.2 with 1mg/ml BSA followed by no more than 10 minutes of rocking at room temperature and was then quickly neutralized by addition of 150 µl of 1M Tris-HCl pH 9.1. The collected solution contained bacteriophage that had survived the first round of biopanning.

The concentration of phage, in units of plaque forming units (pfu) per µl of eluate, was determined using a process called titering, whereby *E.coli (Strain 2738)* was infected with a small amount of phage solution from the eluate and then was spread onto an LB-agar plate and incubated overnight at 37 °C. Because of the presence of a LacZ gene in the M13 genome, *E.coli* colonies infected by phage turn blue on the LB-Agar plates containing IPTG/XGAL. The following day, the number of blue plaques formed on the plate indicated the number of bacteriophage in the eluate. At the same time, 1 ml of the eluate was amplified in an overnight *E.coli* culture diluted in 20 ml LB for 4.5 hours at 37°C followed by purification by centrifugation (Beckman Avanti J-20XP) at 10,000 rpm to remove *E.coli.* An overnight 4°C precipitation of bacteriophage was then performed by addition of 20% (w/v) polyethylene

glycol-8000, 2.5M NaCl at one sixth the volume of the phage supernatant. The phage was isolated by centrifugation at 13,000 rpm and resuspended in TBS (50mM Tris-HCl pH 7.5, 150mM NaCl). The amplified phage was titered for concentration, completing amplification of the first round of biopanning.

The procedure for the second round of biopanning was essentially the same as for the first round with two exceptions. First, phage interaction used the amplified eluate from biopan one in 200 µl of TBST 0.1%, not the original library stock. Secondly, TBST 0.5% was used for the washes to enhance stringency and ensure that only the most strongly attached phage would remain on the luciferase target. In round two of biopanning, following titering of the eluate, twenty plaques were isolated, amplified, and their DNA was extracted using QIAprep Spin M13 Kit (Qiagen) and sent off for sequencing. DNA sequencing was done at the MIT Biopolymers Lab.

In an effort to select for sequences that do not bind luciferase at the substrate binding active site, in the next round of biopanning, an interaction with luciferin, the substrate for luciferase, was included. The motivation is for the luciferin to act as a competitive inhibitor of phage binding to luciferase so that any phage that binds to the active site will be competed off. D-Luciferin was purchased from Sigma and was prepared using the following method. Sterile water (50 ml) was mixed with 15 mg of $NaHCO_3$ and de-oxygenated by alternate vacuum and N_2 flow. Eight hundred microliters of this solution was added to the luciferin and mixed well. Two hundred microliters of additional solution was used to rinse out the luciferin container and then combined with the other 800 µl. The final concentration of the luciferin stock was 1 mg/ml or 3.57 mM. The luciferin stock was then aliquoted into 100 µl fractions and stored at -80 °C. This stock was

then was prepared as a 0.5 mM solution of luciferin in 0.1 M Tris Acetate Buffer pH 7.5. All solutions with luciferin used in the experiments were kept at 4°C in the dark.

For the third round of biopanning, the procedure was the same as for biopan round 2 with the following exception. After phage interaction and the ten washes with TBST 0.5%, there was an additional competition step using 200µl luciferin (0.5 mM in Tris Acetate Buffer pH 7.5). The solution was allowed to incubate, covered with foil, on ice for 30 minutes with rocking. The luciferin competes with phage for binding to luciferase at the active site. The solution was then withdrawn and the target plates were washed six times with Tris Acetate Buffer pH 7.5 0.5% Tween-20 (TABT 0.5% Tween-20). The remaining phage that were still attached to the target plate were eluted using regular pH elution and collected.

Results and Discussion

Table 1 shows phage concentration from titering the eluate, before and after amplification for biopan rounds one through three. The resultant peptide sequences from biopan round 2 are given in Appendix A.

Table 1. Phage Concentrations (pfu/µl) Biopans 1-3. Eluate refers to the collected phage after pH elution and amplified eluate refers to phage after being amplified in *E.coli* for 4.5 hours at 37°C.

	Concentrations (pfu/ul)					
	Biopan 1	Biopan 2	Biopan 3	Luciferin BP3	PL3 Clone	Biopan 3 Repeat
Eluate	480	2530	1.20E+05	2.30E+04		5.30E+05
Amplified Eluate	1.12E+09	2.60E+11	2.70E+11	5.80E+09	1.60E+09	N/A

DNA sequencing for the third round eluate returned one dominant sequence (Figure 13) with a 60% incidence rate from a sample population of 20 – the peptide sequence CKLHGTSRC. The letters represent amino acids and the colors group them into categories based on their R groups:

Acidic (Red), Basic (Blue), Hydrophobic (Orange), Hydroxyl (Green), Ring Groups (Tan), Proline (Yellow), Amide (Purple), and Methionine (White).

One of the clones with the dominant sequence (Sequence 3) was selected for amplification and subsequent ELISA to determine relative interaction strength and this clone was identified as PL3.

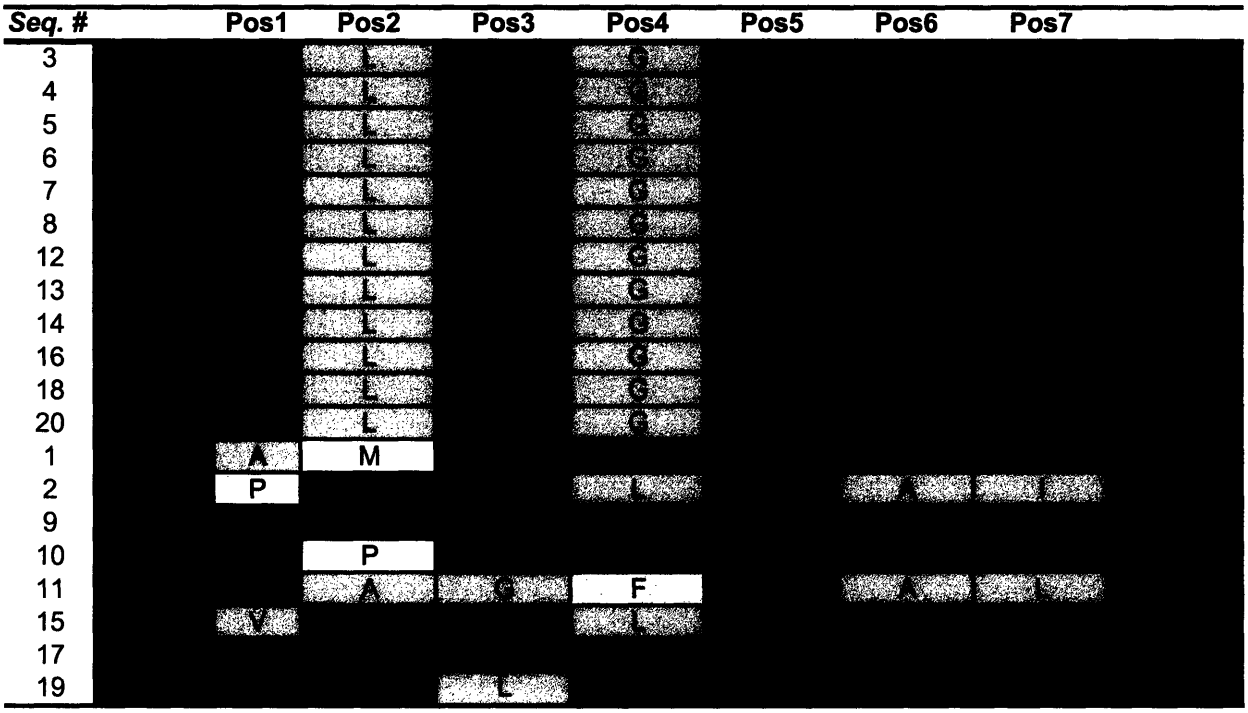

Figure 13. Biopanning Round 3 Phage Eluate Peptide Sequencing Results. The letters represent amino acids and the colors group them into categories based on their R groups: Acidic (Red), Basic (Blue), Hydrophobic (Orange), Hydroxyl (Green), Ring Groups (Tan), Proline (Yellow), Amide (Purple), and Methionine (White). The sequences have been ordered in such a way to highlight the dominant sequence with twelve occurrences out of a total of 20 sequences: CKLHGTSRC. Another sequence that will occur in a subsequent experiment of note is CTKRNNKRC.

There was a predominance of positively charged amino acids (blue) as well as hydroxyl groups (green). The motif KR showed up many times as well as the motif TS or ST. These results showed promise in that these motifs are not likely to interact with luciferase at the active site. The active site is very positively charged (Figure 12), with a Histidine (H), Arginine (R), and

Lysine (K) and our consensus sequences were also mostly positive and therefore likely target another region in luciferase.

2.3.4 Enzyme Linked ImmunoSorbant Assay (ELISA)

Methods

For the ELISA, a 96-well plate was coated with 50 µl of 75µg/ml luciferase in 0.1M $NaHCO_3$ pH 8.6 and allowed to incubate overnight in a humidified chamber at 4°C. The following day, the luciferase solution was removed and the wells were washed three times with 200 µl of TBST 0.1% followed by addition of 200 µl blocking buffer and incubated for 1 hour on a rocker at room temperature. The wells were then washed three times with TBST 0.1% followed by phage interaction. Amplified phage clone PL3 (Sequence 3 from Figure 13) was serially diluted in blocking buffer. Column one was a five fold dilution of the stock phage amplified solution and each subsequent column was a two fold dilution of the previous column (Figure 16). As negative controls, wild-type M13 (M13KE) and p3S1 (streptavidin binding M13 bacteriophage) were included as well as a blank. The stock concentrations of phage are shown in Table 2 and all are at the same order of magnitude.

Table 2. Concentration of Phage for ELISA of PL3 with Controls.

	PL3	M13KE	p3S1
Concentration (pfu/ul)	1.10E+09	2.80E+09	1.30E+09

The phage were incubated on the plate for 1 hour at room temperature with rocking. The wells were washed three times with TBST 0.1%. Horseradish peroxidase (HRP, 200 µl) conjugated to anti-M13 Monoclonal Antibody (Pierce, Rockford, IL) diluted 1:5000 in blocking buffer was

then added to each well and incubated for 30 minutes at room temperature with rocking. The HRP solution was removed and the wells were washed three times with TBST 0.1%. Then 200 µl of 2-2'-azino-di-(3-ethylbenzthiazoline sulfonic acid) solution (ABTS, 0.22 mg for every 1 ml of 0.05 M Citric acid, pH 4.0, stored at 4°C) with 30% hydrogen peroxide (added immediately before use) was added to each well and incubated for 30 minutes at room temperature with rocking.

Results and Discussion

The resultant color change from the ELISA is shown in Figure 14. The high intensity in color corresponding to the PL3 clone, as compared with the low intensities in color of the negative controls (M13KE, p3S1), qualitatively show that the PL3 clone binds better to luciferase than the negative controls do.

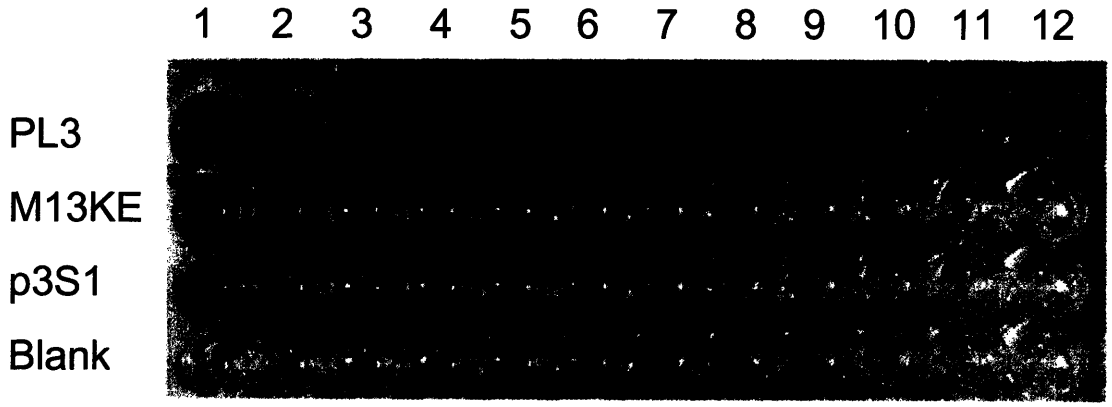

Figure 14. ELISA Results for Clone PL3 and Controls. M13KE is the wild-type M13 phage and p3S1 is the streptavidin-binding phage.

For a more quantitative evaluation of the binding properties, the ELISA plate was read with a fluorescent plate reader (Spectramax Gemini), and the absorbance results were plotted against expected phage concentrations (pfu/µl) from the dilutions (Figure 15).

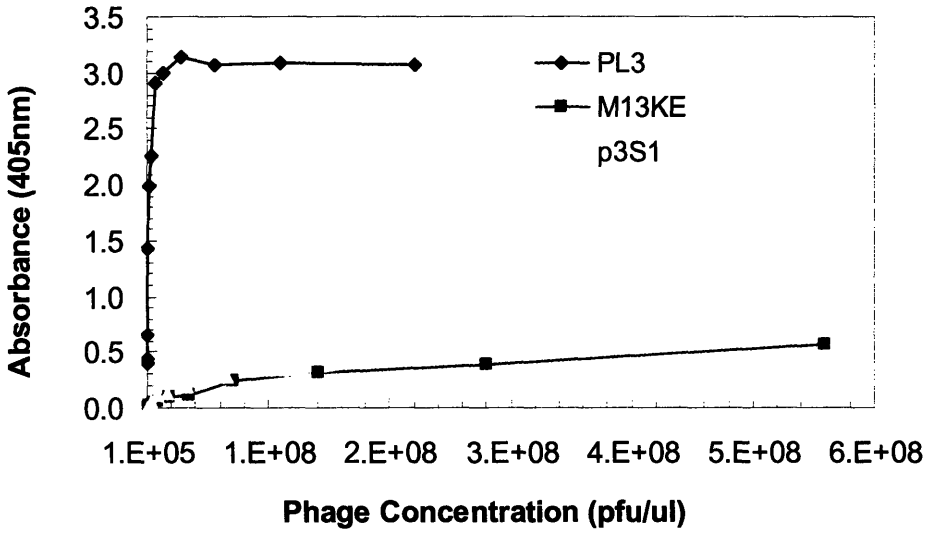

Figure 15. Absorbance VS Expected Phage Concentration From ELISA. M13KE is the wild-type M13 phage and p3S1 is the streptavidin-binding phage. The readings were normalized with a blank subtraction

The sample with clone PL3 had much higher absorbance values than the negative controls, indicating that it bound much better to luciferase than any control phage does. Since wild-type M13 only exhibits non-specific binding, this higher affinity to luciferase shown by clone PL3 can be attributed to specific binding.

2.3.5 Biopanning with Luciferin Competition in Every Round

Methods

Since the previous rounds of biopanning only included the luciferin competition step for the third round, for added rigor, the biopanning was repeated from the beginning, using a luciferin competition step in every round. Four rounds of biopanning (1b-4b) were performed as described previously (procedure for Biopan 3 in Section 2.3.3). Washes following luciferin competition were performed with TABT 0.1% Tween-20 (Biopan Round 1b) or 0.5% Tween-20

(Biopan Rounds 2b-4b). For Biopan Round 4b, one change was made. The concentration of the 30 minute luciferin interaction was doubled (1 mM) to increase the competing luciferin concentration, providing more stringent selection against phage targeted toward the active site.

Results and Discussion

Titering results from biopan rounds 1b to 4b are shown in Table 3.

Table 3. Titering Results from Biopan Rounds 1b to 4b.

	Concentrations (pfu/ul)			
	Biopan 1b	**Biopan 2b**	**Biopan 3b**	**Biopan 4b**
Eluate	450	1.20E+03	3.30E+04	3.20E+05
Amplified Eluate	> 1E+10	> 1E+12	N/A	N/A

DNA sequencing results from biopan rounds 2b and 3b are shown in APPENDIX A and round 4b results are shown in Figure 16.

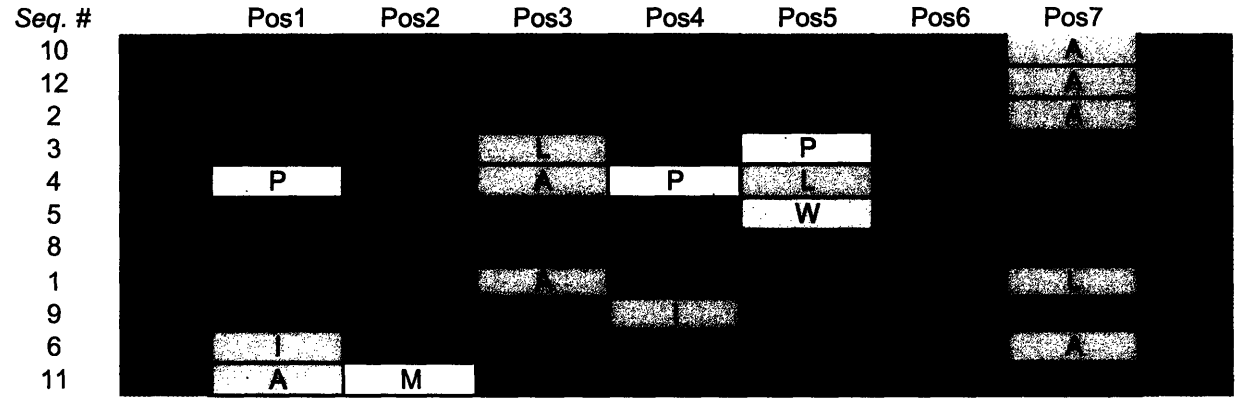

Figure 16. Biopan Round 4b DNA Sequencing Results, Reordered. The letters represent amino acids and the colors group them into categories based on their R groups: Acidic (Red), Basic (Blue), Hydrophobic (Orange), Hydroxyl (Green), Ring Groups (Tan), Proline (Yellow), Amide (Purple), and Methionine (White).

Again, the predominance of positively charged residues (blue) as well as amide groups (purple) of the sequences in Figure 19 leads to the conclusion that the sequence chosen were unlikely to sit in the luciferase active site.

Three phage clones were selected from biopan round 4b as well as two phage clones from biopan round 3 for amplification in *E.coli* for ELISA. They are listed in Table 4.

Table 4. Phage Clones Selected for Amplification for ELISA. Phage clones were selected based on consensus in DNA sequencing results or appearance in multiple rounds.

Clone Number	Sequence	Biopan Round	Seq. #
1	CKLHGTSRC	3	8
2	CTKRNNKRC	3	17
3	CTRHKNQAC	4b	10
4	CAMSQKSTC	4b	11
5	CKKHIRQNC	4b	9

These clones were selected based on high incidence in the biopanning rounds as well as repeats between rounds. The peptide sequence represented by clone 1 had highest prevalence in Biopan Round 3 with 12 occurrences out of 20 sequences and was the same peptide sequence as clone PL3 in Figure 13 and Table 2. Clone 2 was seen both in biopan round 2 and 3. Clone 3 had highest prevalence in biopan round 4b with 4 occurrences out of 10 sequences. Clone 4 was seen cross-biopans – in biopan round 3 and 4b. Clone 5 was seen in both biopan rounds 3b and 4b. These clones were believed to have highest affinity for the substrate luciferase.

2.3.7 ELISA of Selected High Affinity Clones

Methods

ELISA methods followed the same protocol as described in Section 2.3.4. Exact titers for the undiluted phage are given in Table 5. M13KE was used as a negative control and two blanks were included: one with blocking buffer in all wells but no phage, and one without anything except the last step addition of ABTS. After addition of ABTS/H_2O_2, the plate was incubated at

room temperature for 1.5 hours with the ABTS before analyzing with a fluorescent plate reader (SpectraMax Gemini).

Table 5. Concentration of Amplified Phage for ELISA (pfu/µl).

	Clone 1	Clone 2	Clone 3	Clone 4	Clone 5	M13KE
Concentration (pfu/ul)	5.00E+09	4.50E+09	2.45E+09	2.50E+09	1.00E+09	2.80E+09

Results and Discussion

The resultant color change from the ELISA is shown in Figure 17. The high intensity in color corresponding to the Clones 1-5, as compared with the low intensities in color of the negative controls (M13KE, Blank), qualitatively show that the selected clones bind better to luciferase than the negative controls do.

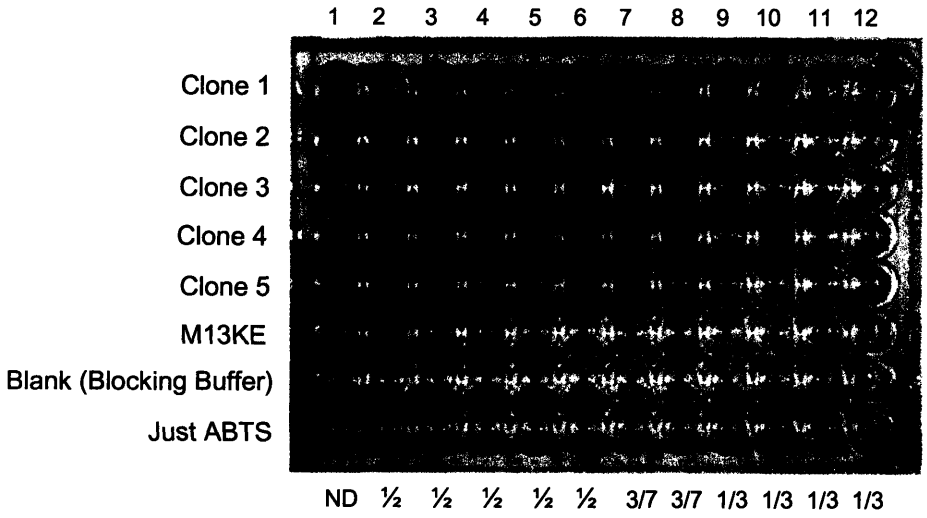

Figure 17. ELISA Well Schematic and Results for Amplified Clones 1-5. The dilution factors on the bottom are with respect to the previous well and ND represents No Dilution.

Figure 18 shows the results of the ELISA measurements and Figure 19 is a magnified version of Figure 18, expanding the area of exponential increase.

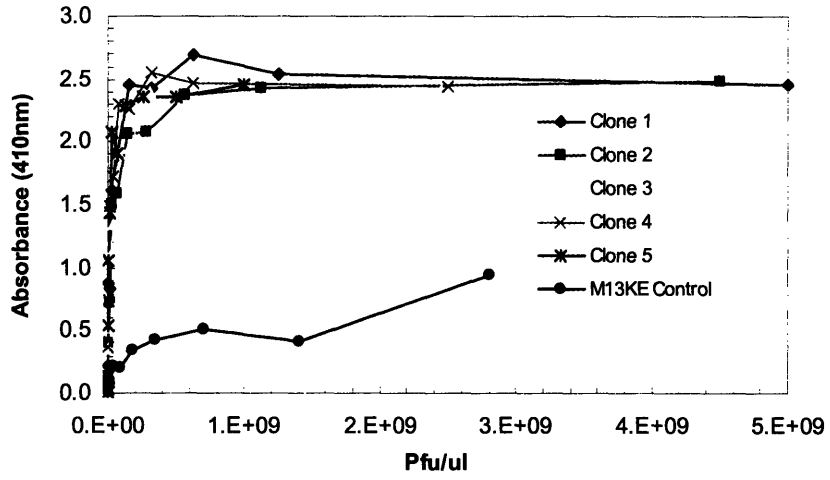

Figure 18. Luciferase ELISA with Clones 1-5 and M13KE Control.

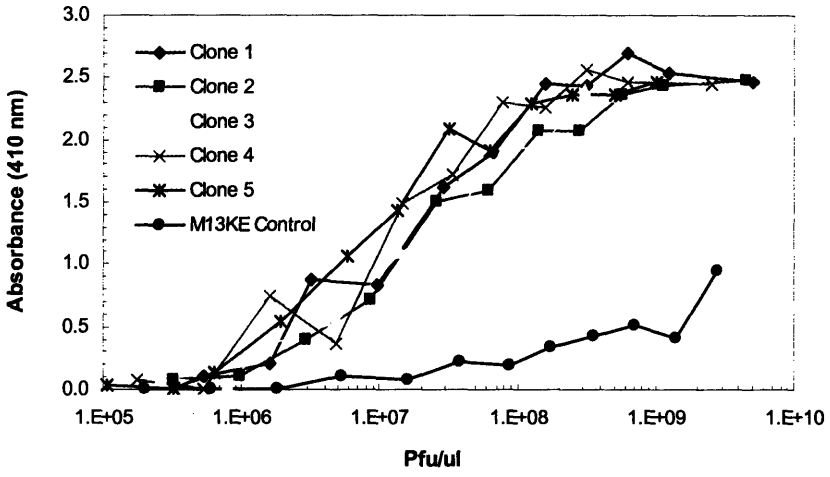

Figure 19. Luciferase ELISA of Clones 1-5 with M13KE Control. This graph is focused on the exponential growth phase of the curves from Figure 18.

The absorbance values of the five selected phage clones were relatively similar but were an order of magnitude above that of the negative control (M13KE). The results revealed that all the selected clones from phage display have much higher affinity for luciferase than wild-type phage.

2.3.8 Large Scale Amplification

Methods

Clones 1 and 3 were selected for large scale amplification to produce liquid crystalline phage films. Phage was amplified in a 1 liter LB/*E.coli* culture for 6 hours in a 37°C shaker followed by centrifugation at 10,000 rpm remove bacteria. The phage was precipitated overnight at 4°C with addition of 20% (w/v) polyethylene glycol-8000, 2.5M NaCl at one sixth the volume of the phage supernatant. The phage was then isolated by centrifugation at 13,000 rpm, resuspended in 1 ml of TBS, titered, and DNA sequenced. The large scale amplification was repeated three times to obtain enough phage.

Results and Discussion

DNA sequencing of amplified clones 1 and 3 resulted in the sequences CKLHGTSR and CTRHKNQAC, respectively, verifying purity of the amplifications. Amplification titers are shown in Table 6.

Table 6. Titer Results from Large Scale Amplifications of Clones 1 and 3.

	Concentrations (pfu/ul)			
	Amp 1	**Amp 2**	**Amp 3**	**Amp 4**
Clone 1	1.6E+10	5.0E+09	7.2E+09	5.0E+09
Clone 3	2.5E+10	2.5E+08	1.3E+09	3.0E+09

Concentrations were converted from pfu/ul to mg/ml using Beer's law (Eq.1):

$$A = \varepsilon l c, \qquad \text{(Eq. 1)}$$

where A is the absorbance, ε is the molar absorptivity or extinction coefficient, l is the cell path length, and c is the concentration. The path length was 1 cm. Following from Beer's Law, the concentration of phage was calculated in mg/ml (Eq. 2):

$$\text{mg/ml} = \frac{(Ab_{269} - Ab_{320}) * \text{DilFact}}{\varepsilon}, \qquad \text{(Eq. 2)}$$

where Ab_{269} is the absorbance at 269 nm, Ab_{320} is the absorbance at 320 nm, DilFact is the dilution factor of the phage solution, and ε is the extinction coefficient which for phage at this wavelength and cell path length, is 3.84 (33). For all of our calculations, the dilution factor was 50.

The concentration of phage was also calculated in units of phage/ml in Equation 3:

$$\text{phage/ml} = \frac{(Ab_{269} - Ab_{320}) * 6 \times 10^{16}}{\#\text{bp} + \#\text{nucleotide}}, \qquad \text{(Eq. 3)}$$

where for the M13 bacteriophage, the number of base pairs is 6,400 and the number of nucleotides on the plasmid is 822.

2.3.9 Luciferase Activity Assay Methods

Luciferase signal was determined using the Promega Bright-Glo Luciferase Assay System and a Turner Biosystems Veritas Microplate Luminometer. For the film experiments, Promega Quantilum Luciferase was used.

2.3.10 M13 – Luciferase Films

Methods

Based on enhanced protein stability (38-40), 5% sucrose was added to half of the virus-based film samples. Twenty samples were prepared for each condition listed in Table 7 with the exception of luciferase (L) which had 22 samples and M13KE which had 11 samples. A total of 270 samples were prepared.

Table 7. Luciferase Phage Film Conditions and Samples.

Drying at 4 degrees C	Drying at Room Temperature
Clone 1 + Luciferase (C1)	Clone 1 + Luciferase (C1)
Clone 1 + Luciferase + 5% Sucrose (C1S)	Clone 1 + Luciferase + 5% Sucrose (C1S)
Clone 3 + Luciferase (C3)	Clone 3 + Luciferase (C3)
Clone 3 + Luciferase + 5% Sucrose (C3S)	Clone 3 + Luciferase + 5% Sucrose (C3S)
M13KE(chiang) + Luciferase (M)	
M13KE(chiang) + Luciferase + 5% Sucrose (MS)	
Luciferase (L)	Luciferase + 5% Sucrose (L)
Luciferase + 5% Sucrose (LS)	Luciferase + 5% Sucrose (LS)

For each sample, phage concentration was kept at 6 mg/ml and luciferase concentration was maintained at 22.8 µg/ml to create a 1:1 ratio of phage to luciferase. Sucrose was prepared in TBS and was added at 5% w/v for the appropriate samples. The volume of each sample was approximately 20 µl. The samples were prepared in eppendorf tubes and the tubes were placed, with the caps open, in Tupperware containers containing desiccant. Due to the deleterious effects of vibrations on film integrity and uniformity, the containers were sealed, placed in secondary boxes, and kept at 4°C on an anti-vibration platform or at room temperature in a reduced vibration room.

Results and Discussion

The samples stored at room temperature took 6 days to dry and the samples stored at 4°C took over two weeks to dry. A sample of the virus film with luciferase was analyzed using SEM (Jeol 6320 FV) (Figure 20).

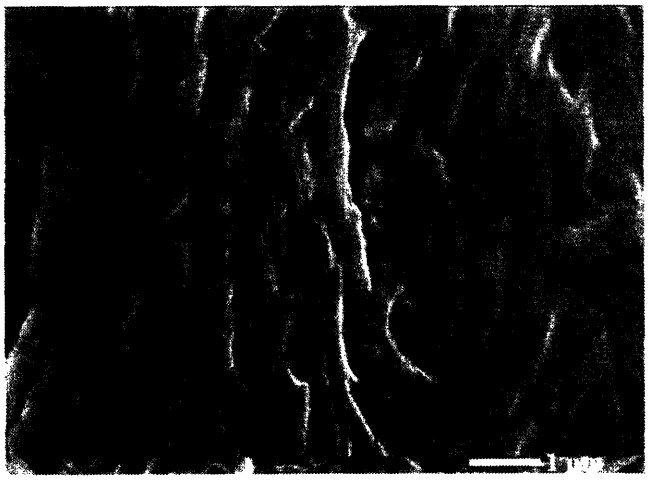

Figure 20. M13 Virus Film with Luciferase. SEM Image (Jeol 6320 FV)

Upon analysis of the films assembled, several abnormalities became apparent. First, unlike the film behavior seen in the past (14), films synthesized with luciferase were difficult to separate from the eppendorf tube. The film appeared to be extremely brittle. Increasing the volume as well as phage concentration of the samples may overcome this problem. Additional observations included a reduced luciferase signal intensity of the dried film, which could be attributed to one of two reasons. First, the luciferase could be so well encapsulated within the film that it was not accessible to its substrate, luciferin, and thus the interaction needed to produce the luminescent reaction could no longer happen. Second, during the drying process, the luciferase may have migrated to the surface of the film and therefore was exposed on one side, allowing it to move

more freely and possibly denature. The physical integrity of the film appeared to be very strong and even sonication of the film in TBS buffer failed to dissolve the film. Whether this integrity translates to stability of the luciferase would still need to be investigated. Possible solutions to dissolve the film without compromising the integrity of the luciferase include alternate dissolution buffers, cell culture media, and LB.

Another challenge is to control edge effects when drying the film so as to maintain a uniform structure as well as phage/luciferase concentration throughout the film. Higher pressure systems can be investigated, though it is possible that could increase drying time.

2.4 Conclusions and Future Work

The potential of long term storage of protein-based vaccines at room temperature or elevated temperatures by 3-dimensional structural control in M13 virus films would be a tremendous step in obviating the need for the cold chain. From the experiments done thus far, a model protein was chosen and sequences of peptides expressed on M13 bacteriophage that can bind to the protein were identified, and luciferase-phage films were created. The next steps would be to find a way to release the protein and measure its activity after various time points ranging from 30 minutes to 4 months or longer to determine shelf life. In addition, studies at elevated temperatures (25°C - 40°C) will also need to be conducted to establish feasibility of using this storage method in tropical regions of the world.

CHAPTER 3 - Virus-Based Multifunctional Platform for *in vivo* Cancer Diagnostics

3.1 Abstract

In an effort to detect tumors before they turn into late stage cancer, researchers have turned to various imaging modalities and diagnostic probes, including fluorescent and magnetic nanoparticles specific for tumor markers. The aim is to create a sensitive, accurate, and clear image of the tumor-affected regions. Most of the research, however, focuses on functionalized single nanoparticle systems. Our research brings a unique spin to the arena by proposing to designing a multi-particle and multi-functional system based on the M13 bacteriophage. We are using the bacteriophage as a bigger and brighter marker for cancer lesions. M13 bacteriophage has the advantage in that it is composed of 2700 copies of a major coat protein (p8) and 5 copies of a minor coat protein (p3) that can be genetically engineered to express peptides that have high affinity for cancer markers, other proteins, and inorganic materials. The multiple copies of the coat proteins lend themselves to high avidity interactions. Methods such as biopanning or cloning can be used to engineer phage that can bind to cancer target as well as imaging modalities such as quantum dots and magnetic nanoparticles. The tri-fold capability to target a lesion and image both fluorescently and magnetically would provide ease and flexibility to cancer imaging. Additionally, the capacity to have thousands of copies of the targeting sequence on our M13 bacteriophage probe could possibly increase the sensitivity of detection and catch lesions that previously went unnoticed. This sensitivity enhancement would be of significant help in the detection of cancers like breast cancer where traditional mammography has a miss

rate of 10-15%, and in colon cancer, where traditional colonoscopy can only reliably detect lesions greater than 1 cm in diameter. (41) This virus-based multifunctional platform can conceivably be extended to any applications that can benefit from directed targeting and imaging. In addition, once specific diagnosis is achieved, the platform can also be used for directed treatment of the cancer lesions.

In this present study, a 100% expressed p8 library was created for screening against potential cancer markers and work will soon proceed with screening against several cancer cell lines. In addition, a Type 83 phage was created that had a sequence directed against vascular cell adhesion molecule-1 (VCAM-1) expressed on the p3 and a tri-glutamate sequence (E3) on the p8 that can bind well to positively charge molecules like amines. Lastly, successful attachment of amine-terminated CdSe/ZnS quantum dots to p8E3 phage (E3 on p8 and wild type on p3) was performed and III-Vquantum dots (GaN and InN) were water solubilized for use *in vivo*.

3.2 Introduction

3.2.1 Phage in Medicine

Phage was discovered in the early 1900s, and since then, have been used in medicine in a variety of ways, establishing itself as a jack of all trades. (42) In this chapter, an application of the M13 bacteriophage in the sector of imaging and cancer diagnostics will be described. However, first, a few ways phage has been used in medicine in the past will be examined.

Phage can be and has been used in medicine anywhere from prevention to diagnosis to treatment. In the prevention of disease, phage has been used as vaccine delivery vehicles (43, 44). Recently, it was shown that unmodified phage can be used to deliver DNA vaccines more efficiently than standard plasmid DNA vaccination (43, 45-47). Phage display has also been used to identify potential vaccines (23, 48).

In the diagnostics sector, phage have been used for decades in detection and typing of bacteria. (49-52). Phage display technology has been used for detection of biological threat agents (53), as well as bacteria and viruses like botulinum toxin (54), hepatitis C (55, 56), human cytomegalovirus (57), rabies virus (58), vaccinia virus (59), ebola virus (60), and anthrax spores (61).

Phage has been used in gene therapy (62), with targeting sequences expressed on the phage to direct them to cells with correct receptors (63, 64), using both artificial covalent conjugation and phage display. Examples include integrin-binding peptides (65) and DNase II inhibitors to reduce DNA degradation (66). Phage has also been manipulated for tissue targeting (67-69) and creating landscape phage which are collections of phage clones with diversified surfaces composed of random peptide libraries fused onto the phage (70-72).

Lastly, phage has been used in the treatment of infections and other diseases, such as the multi-drug resistant *Pseudomonas* infection in Figure 21 which had failed to heal after one year of conservative wound care management, but healed within two weeks by phage therapy. (45)

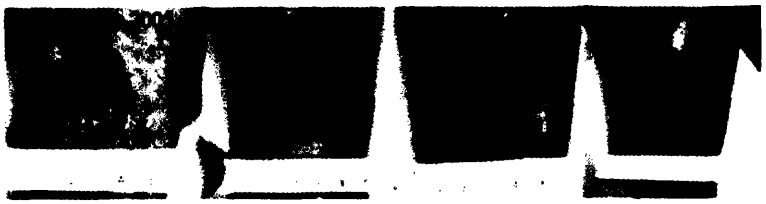

Figure 21. Venous Leg Ulcer from Multi-Drug Resistant Bacterial Infection Successfully Treated with Phage. Pictures reproduced, with permission, courtesy of Dr. Randall Wolcott, Southwest Regional Wound Care Center, Texas. (45)

Lytic phage have been used as antibacterials because they are more specific than normal antibiotics due to their specific bacterial host tropism (73). In a recent study, T4 phage was orally administered to human volunteers to treat *E.coli* caused diarrheal disease (74). Phage has also been used to treat something as diverse as cocaine addiction due to the ability of the phage to cross the blood brain barrier and penetrate the CNS when administered intranasally (75).

Table 8 below gives additional examples on how phage have been used in technology or medicine. In addition, human phage therapy trials from Poland and the Soviet Union are included in the APPENDIX B for reference (76). Phage are quite versatile and the potential for more applications is virtually unlimited.

Table 8. Examples of Applications of Phage Therapy in Technology and Medicine. (45)

Application	Advantages	Disadvantages
Decontamination of surfaces and/or environment	Can kill antibiotic-resistant bacteria	Not as broad spectrum as other decontaminants Effective life span is limited
Carcass treatment	Specific food-poisoning bacteria can be targeted	Potential regulatory problems if used with food products
Plants	Few regulatory problems expected. Phage shouldn't be specifically inactivated Can treat specific diseases	Potential problems with non-specific phage inactivation due to environment
Aquaculture	Can potentially be delivered in feed Phage neutralizing antibodies do not seem to be produced in fish	Might need to administer phage continuously or relatively soon after infection More studies are needed
Phage therapy in	Fewer regulatory hurdles	Needs to be proven in large-scale studies

Application	Advantages	Disadvantages
animals	Can reduce the use of antibiotics Multiple delivery routes have been tested	Probably not applicable for long-term treatments (e.g. where broad-spectrum antibiotics are used to enhance growth)
Humans: oral	Easy to deliver Potential to deliver in food and/or drink. Highly specific, therefore will not damage gut flora	Might need to neutralize stomach acid High levels of endotoxin can be produced from lysed bacteria
Humans: intravenous	Spreads rapidly throughout the body	Phage swiftly cleared by the immune system but new data may show that not to be true (Weissleder's Group)
Humans: topical	Multiply *in vivo* Can treat antibiotic-resistant infections *In vivo* amplification of phage can enable them to penetrate into wounds Phage can produce enzymes to break down biofilms enabling access to pathogens Can be delivered conveniently (e.g. in creams, rinses and patches)	Phage need to be highly purified Might need continuous treatment with low levels of phage Interference by the host immune system

3.2.2 Phage Advantages and Disadvantages for Cancer Diagnostics

The aim of the research presented here is to use the M13 bacteriophage as a platform on which to combine cancer marker targeting sequences with imaging units such as quantum dots or magnetic nanoparticles. Phage present many attractive features. For one, the M13 bacteriophage has a high surface area or surface density (300-400 m^2/g), better than the best-known absorbents and catalysts (53). In this respect, the phage is a like a viral adhesive that can stick to whatever it has been designed to target. Furthermore, a phage has 2700 copies of the major coat protein p8, and this creates a high avidity system, which when combined with high affinity interactions between the cancer targeting peptides expressed on the phage and the cancer lesion, creates a system for more sensitive and specific detection. The phage is also a multifunctional system due to its many different coat proteins, which can all be engineered to carry different units, either peptides or inorganic imaging motifs.

The phage is also very robust structurally. It is resistant to heat (77), many organic solvents (78), urea (up to 6M), acid, alkali, and other stresses (53). Biologically, phage are not phagocytosed well by mammalian macrophages and therefore have a good chance of arriving at the tumor sites. Studies with *in vivo* phage panning has shown that there are no deleterious effects with phage injection, the immune response is low, and the phage can circulate in the bloodstream long enough to reach their tumor targets (79). Additionally, due to their small size, especially along the minor axis, phage are small enough to slip through endothelial walls of the vasculature and extravasate into tumor sites, eliminating the need for complex chemistry to enable the extravasation. While phage, just as with many foreign bodies, can be cleared via the reticuloendothelial system, thereby decreasing the concentration of phage reaching the tumor targets and reducing the effectiveness of phage diagnostics or therapy (45, 76), some studies have shown that to not to be a major problem. *In vivo* experiments showed that phage can remain in the body for a prolonged time (ie. several days) (76, 80).

3.2.3 Breast Cancer

For our initial cancer target, breast cancer was chosen due to the pressing global health need for early detection. Breast cancer is the second leading cause of cancer deaths in women today (after lung cancer) and is the most common cancer among women, excluding non-melanoma skin cancers. According to the World Health Organization, more than 1.2 million people will be diagnosed with breast cancer this year worldwide. The American Cancer Society estimates that in 2005, approximately 211,240 women in the United States will be diagnosed with invasive breast cancer (Stages I-IV). The chance of developing invasive breast cancer during a woman's lifetime is approximately 1 in 7 (13.4%). Another 58,490 women will be diagnosed with *in situ*

breast cancer, a very early form of the disease. In addition, breast cancer also occurs in men. An estimated 1,690 cases will be diagnosed in men in 2005. About 40,410 women and 460 men will die from breast cancer in the United States this year. (81)

While mammograms are considered the gold standard for breast cancer detection, 10 to 15 percent of all breast cancers are not detected by a mammogram. A careful clinical breast examination is also necessary. A palpable breast mass that is not seen on a mammogram should have a thorough diagnostic work-up including ultrasound and needle biopsy and close follow-up (41). Other diagnostic techniques include ultrasonography, which is not to be used for routine screening, primarily because microcalcifications are not visualized and the yield of carcinomas is negligible (82).

Tumour progression and the development of metastases involves several steps that include uncontrolled cell growth, loss of homophilic intercellular interactions, migration of tumour cells into vessels or lymphatics, interaction with surface constituents of platelets and leucocytes, adhesion to lymphatic or vascular endothelium at distant sites, migration into the parenchyma, induction of neoangiogenesis, and cell growth (83-85). In breast cancer, metastases tend to migrate to the bone or the lung (86) with primary visceral metastases having a worse prognosis than primary bone metastasis, where the former has a survival time of only 9 months while the latter survival time is around two years (87). Between 60% and 70% of women who die from breast cancer have lung metastases. In 21% of cases, the lung is the only site of metastasis (81).

Vascular cell adhesion molecule-1 (VCAM-1) plays a role in cell adhesion to the vascular endothelium, and may have a role in tumor cell dissemination. The prognostic value of the adhesion molecules was examined in a study by O'Hanlon et al. In patients with Stage 2 disease,

elevated VCAM-1 was predictive of decreased survival, even when corrected for T and N status. (T and N refer to tumor size and nodal metastases and are part of the TNM staging criteria for evaluating cancers). Adhesion molecules are elevated in patients with advanced disease, and elevation in VCAM-1 has prognostic significance in patients with breast carcinoma (88). Interestingly, for the research presented here, peptides with affinity for VCAM-1 have been found via p3 phage library screening (89).

3.2.4 Virus-Based Cancer Detection Platform

The focus of the research presented here is on diagnostic medicine with the potential to extend to treatment. The M13 bacteriophage serves as the foundation of the proposed cancer detection device. Due to its multifunctionality via its various coat proteins, there is tremendous potential in expressing various cancer detecting peptides onto the ends of the coat proteins by way of either library phage selection or direct engineering of the genome. In addition, the ability to perform phage selection on both the p3 and p8 allow for identification of phage that can serve as a holder for nanoparticle that will label its surface. Therefore, the project is divided into two discrete sections: 1) Cloning or attaching the Cancer Targeting Peptide (CTP) and 2) Attaching nanoparticles. Figure 22 shows the general idea of the proposed system, where the cancer cell receptor is merely a receptor or protein that is up-regulated in particular types of cancers and has been established as a marker for that type of cancer – for example, the VCAM-1 Receptor for Breast Carcinoma.

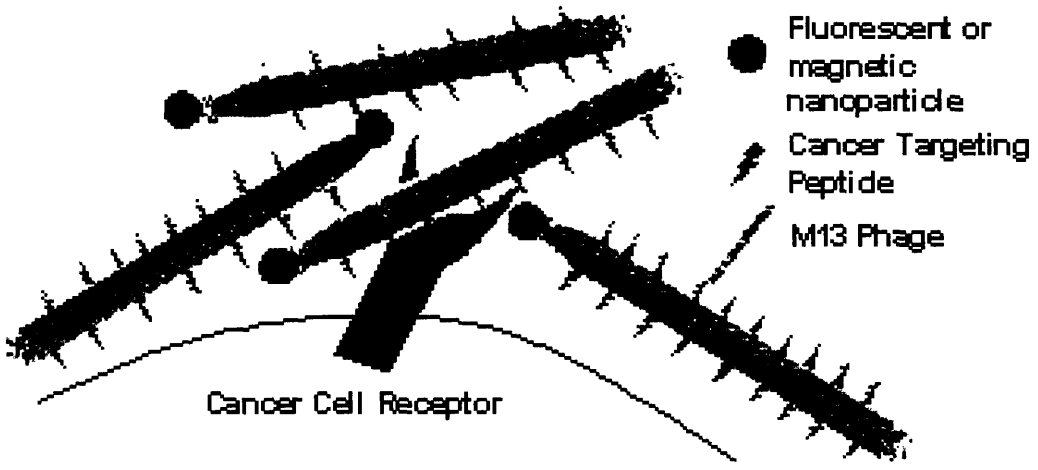

Figure 22. Virus Based Platform for Detecting Cancer. The cancer cell receptor is merely a receptor or protein that is upregulated in particular types of cancers and has been established as a marker for that type of cancer – for example, the VCAM-1 Receptor for Breast Carcinoma. The Cancer Targeting Peptide (CTP) can also be interchanged with the nanoparticle so that the CTP is on the p3 and nanoparticle is on the p8.

There are two methods for inserting the CTP onto the M13 bacteriophage. The first method is to create a site in the phage genome for direct insertion of a peptide sequence that is known to have an affinity for that particular type of cancer. The other method is to screen the target receptor with a phage library. This can be done with either a p3library (commercially available through NEB) or with a p8 library. In both cases, the peptides are directly expressed through the genome.

Two methods will be used to attach nanoparticles to the phage. First, a series of phage selection experiments will be performed, similar to that for luciferase in Chapter 2, to isolate a phage that has selective affinity for the nanoparticles. Alternatively, the coat proteins will be manipulated directly to attach nanoparticles.

Lastly, for *in vivo* applications for colon cancer detection, during a routine colonoscopy, the physician would inject the colon-cancer detecting phage solution and using MRI, can see small

lesions pinpointed on the imaging screen. In the case of breast carcinoma, the *in vivo* applications would involve injection of the phage into the vasculature. In both cases, the solution would be allowed to circulate for some time in order to reach the tumor sites, and again, the sites would be imaged using MRI.

3.3 Methods, Results, and Discussion

3.3.1 Genetic Engineering of M13 Bacteriophage

The work described below is mostly for detection of breast carcinomas, working primarily with the VCAM-1 peptide.

3.3.1.1 Type 8 Phage Library (34) in collaboration with Soo-Kwan Lee

Methods

One method for attaching Cancer Targeting Peptides to the major coat of the M13 bacteriophage was to create a Type 8 Phage Library and screen against cancer targets to find peptides that have affinity for the given cancer lesions.

The M13KE phage vector was modified into the M13SK by making a cloning site for pVIII peptide display (APPENDIX C). A *Pst* I restriction site was made by mutating T to A at position 1372, a *Bam*H I site was made by mutating C to G at position 1381, and the *Pst* I site at position 6246 was deleted by mutating T to A at position 6250. The site-directed mutagenesis was done using overlap extension PCR. A dsDNA library of oligonucleotides was then prepared and cloned into the resulting modified phage vector, named M13SK, using *Pst* I and *Bam*H I. To obtain the dsDNA library, partial library duplexes were formed by annealing of extension primer

(5'- GATGCTGTCTTTCGCTGCAG-3') with oligonucleotides (3'-ACGACAGAAAGCGA CGTCnm(nnm)$_6$nnCCTAGGAACATC ATC-5', where n = A, T, C, or G and m = A or C). The oligonucleotides were purchased from Integrated DNA Technologies, Inc. The partial library duplexes were incubated with Klenow fragment (3'→ 5' exo$^-$) (10 U/µl) and dNTP at 37°C for 30min. The Klenow fragment was inactivated by heating (75°C for 20 minutes), and the mixture was digested with *Pst* I and *Bam*H I. The digested DNA was gel purified (2-40% TBE polyacrylamide gel) (Figure 23), ligated into M13SK, and transfected into XL1-Blue Electroporation Competent Cells using a MicroPulser™ (Biorad) (Figure 24). The phage library was titered and sequenced (MIT Biopolymers Laboratory) before amplification. Detailed protocol for library construction is included in APPENDIX D.

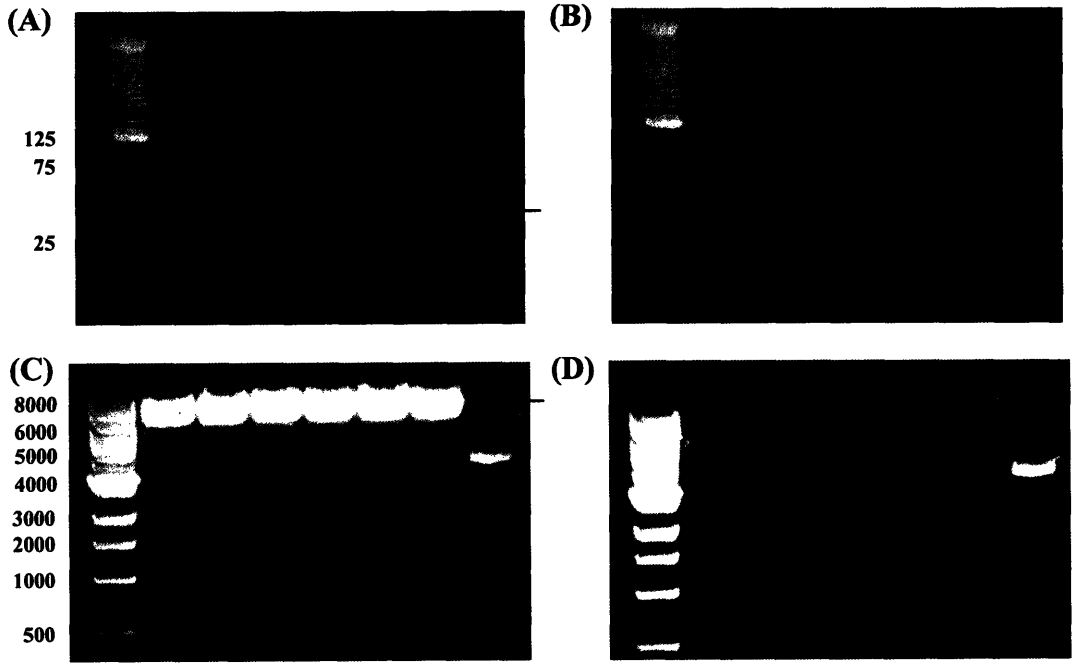

Figure 23. Polyacrylamide Gel (2-40% TBE polyacrylamide gel) Purification of Random Oligonucleotide Insert and M13SK Vector in Preparation for Ligation. The arrows indicates bands of interest. And numbers to the left of the gels are in units of base pairs. **(A)** Digested insert gel **(B)** After removing digested insert band **(C)** Vector, where the last column is the undigested vector which still retains the circular RF form **(D)** After removing digested vector band.

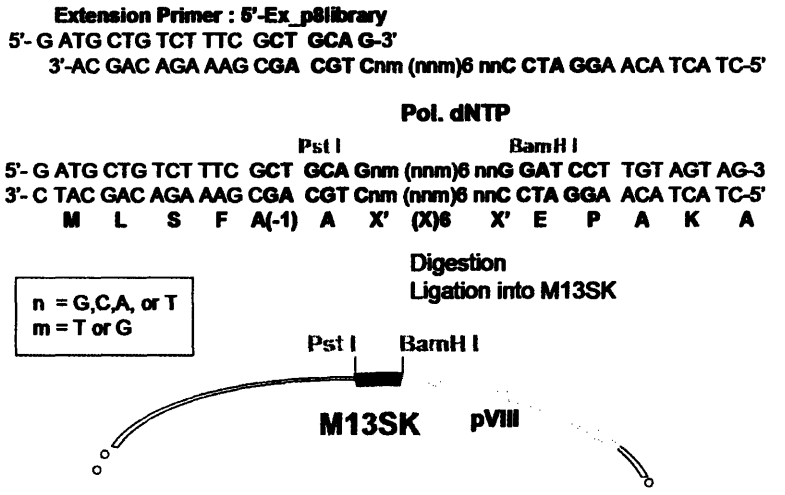

Figure 24. Schematic for Construction of Type 8 Phage Library in M13SK. Schematic shows the restriction sites for cloning DNA library into M13SK. X = any randomized amino acids. (34)

Results and Discussion

Sample sequences obtained from the p8 library construction are given in Table 9 and the diversity was calculated by counting the total number of phage produced by the *E.coli* following electroporation during the 30 minutes incubation period prior to large scale amplification. Diversity was calculated to be around 10^5 phage.

Table 9. Example Peptides from Type 8 M13 Phage Library

Example peptides from Type 8 Phage Library	
GSTDSVSG	AASAELGA
GMADTAST	ENGLTTGA
GEFAPMST	MLRRVSCR
GGVYGAV	GPAVPSFA
RAGAFAGF	EETLPVLP
ENLTTVVS	GAPTEPLP
EVWSAGSE	AGISADLT
EVSTLSNE	AGSATADS

As described in Lee (2006) (34), certain amino acids were more prevalent than others in p8 libraries. For example, basic amino acids were rarer than acidic amino acids. The bias in the type of amino acids able to be incorporated into the p8 was presumably due to the compatibility of electrostatic and structural change with phage major coat protein assembly.

The constructed p8 library could be used to biopan against VCAM-1 to find a peptide that could specifically bind VCAM-1.

3.3.1.2 Type 83 Genetic Engineering in Collaboration with Chung-Yi Chiang

Type 83 Genetic Engineering allow for two different combinations of CTP and nanoparticles. One can either attach the CTP to the p3 and nanoparticles to the p8 or vice versa. In the following experiments, the former was done. Type 83 Genetic Engineering, two inserts were introduced into the genome, one before the gIII and the other before the gVIII, each with different restriction enzyme sites (Figure 25).

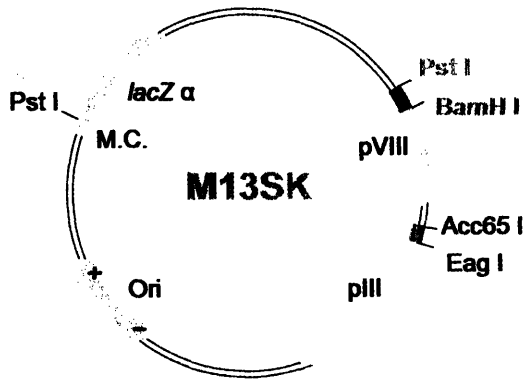

Figure 25. Type 83 Genetic Engineering of M13 Bacteriophage. See also Appendix C.

In the laboratory, two types of Type 8 phage were used, one with a gold binding sequence and the other with several negatively charged glutamates. The first sequence was found by

biopanning against gold using a p8 library (34). The expressed serine-rich peptide sequence was Val-Ser-Gly-Ser-Ser-Pro-Asp-Ser (VSGSSPDS) and the phage was named p8#9 (Figure 26). The second phage clone was a quadruple glutamate sequence (EEEE) sequence called p8E4 which, through multiple amplifications, spontaneously mutated to a triple glutamate (EEE) called p8E3 (Figure 27).

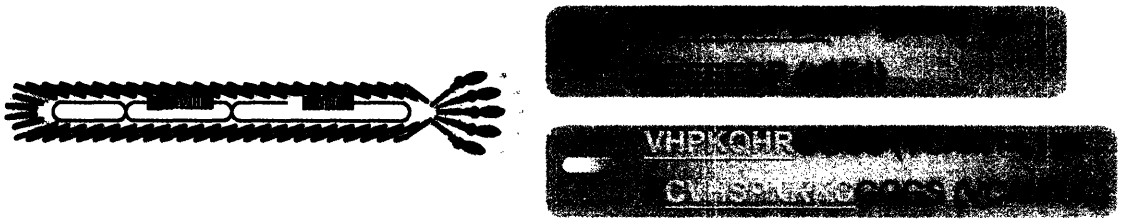

(Kelly, KA. Circ Res. 96, 2005)

Figure 26. P8#9 and P8E4 Type 8 Bacteriophage Combined with VCAM1-Linear and VCAM1-Cyclic Sequences on pIII.

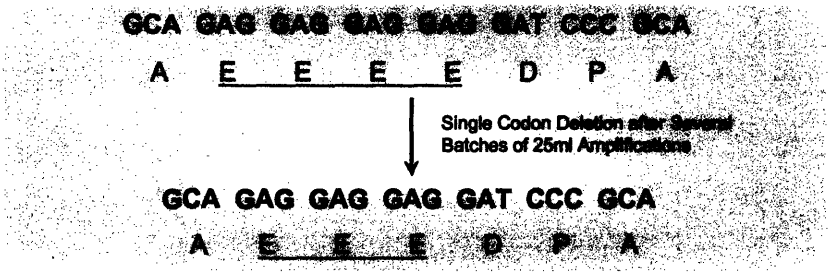

Figure 27. P8E4 Mutation. Spontaneous mutation of p8E4 phage to p8E3 phage through deletion of one glutamate.

Genetic engineering of the p3 site to insert the VCAM-1 sequences was done with standard cloning methods similar to that for p8 random library construct. Oligonucleotides were obtained (5'- CAT GTT TCG GCC GAA CCT CCA CCC CGA TGC TGC TTA GGA TGA ACA GAG TGA GAA TAG AAA GGT ACC CGG G-3') for the linear 7-mer VCAM-1 sequence and (5'-

CAT GTT TCG GCC GAA CCT CCA CCG CACC TTC TTA TTA GGA CTA TGA ACA CAA GCA GAG TGA GAA TAG AAA GGT ACC CGG G-3') for the constrained cyclic 7-mer VCAM-1 sequence from Integrated DNA Technologies (Coralville, IA). The single-stranded oligonucleotides were then extended with the p3 extension primer purchased from NEB (Ipswich, MA), restriction digested with Acc65 I and Eag I, and inserted into the p3 cloning sites of the M13SK vector obtained from p8#9 or p8E3 RF DNA. Isolation of the RF DNA was done by amplifying p8#9 or p8E3 phage in *E.coli* and isolating the RF DNA from the *E.coli* using QIAprep Spin Miniprep Kit.

3.3.1.3 Type 8 Directed Genetic Engineering

Methods

As an alternative to screening for a VCAM-1 binding peptide via p8 library phage screening, direct cloning of the VCAM-1 binding peptide found via p3 library screening (89), into the p8 gene was also tested. The sequences found were either a cyclic 7-mer (CVHSPNKKC) or a linear 7-mer (VHPKQHR).

Because p8 is a structural protein while p3 is not, there is more flexibility in the type of sequence that can be inserted into the p3 than the p8. For p8, often upon insertion of a given sequence, the phage could no longer be packaged due to structural instability resulting from the additional amino acids. In order to achieve 100% display in all p8 copies, only linear sequences were inserted into the p8 genome.

Despite the presence of several positively charged amino acids in the VCAM-1 linear sequence (VHPKQHR), cloning the sequence into the p8 section of the genome was attempted, with and without an extra glycine at the C terminus to act as a flexible linker between the peptide sequence and the p8 coat.

Oligonucleotides were obtained (5'- CTA CTA CAA GGA TCC CCC CGA TGC TGC TTA GGA TGA ACT GCA GCG AAA GAC AGC ATC -3') for the VCAM-1 linear sequence with a glycine linker at the C-terminus and (5'- CAT GTT TCG GCC GAA CCT CCA CCC CGA TGC TGC TTA GGA TGA ACA GAG TGA GAA TAG AAA GGT ACC CGG G-3') for the VCAM-1 linear sequence without a glycine linker.

The oligonucleotides were extended using the same extension primer as that for the pVII8 library cloning (Section 3.3.1.1). Then, the oligos were restriction digested with *Pst* I and *BamH*I, then inserted it into the M13SK genome, followed by transfection into *E.coli*.

Results and Discussion

The results showed that this particular sequence was not able to be taken up by the M13 genome, confirmed by the hypothesis that the large number of positive amino acids disrupted the stability of phage packaging. Therefore, for VCAM-1, the best possibility for attaching the sequence to p8 would be to directly screen against the p8 library and find an alternative peptide sequence that can bind specifically to VCAM-1.

3.3.2 Imaging Modalities

3.3.2.1 Quantum Dot Basics

Conventional fluorescent imaging with organic fluorophors has many shortcomings such as short lifespan, dimness, photobleaching, and difficulty in distinguishing it from cellular auto-fluorescence (90).

Quantum dots have recently been developed and provide a better alternative to organic fluorophors in many ways. Quantum dot fluorescence have a longer lifetime because the quantum dots are resistant to bleaching (90). Furthermore, the fluorescence is typically brighter (90, 91). Only a few dots are needed for signal detection (90, 92), and the signal from the quantum dots have a longer lifetime than the background fluorescence found in a cell; therefore, their emission is easily distinguishable (93).

Quantum dots are semiconductor nanostructures from about 2 to 50 nanometers in size that confine the motion of conduction band electrons, valence band holes, or excitons (pairs of conduction band electrons and valence band holes) in all three spatial directions, resulting in a change of electronic or optical properties as compared to bulk materials. A quantum dot has a discrete quantized energy spectrum, and it is from this energy spectrum that arise the coloration of quantum dots. The band-gap energy of the fluoresced light is inversely proportional to the square of the size of the quantum dot. Larger quantum dots have more energy levels which are more closely spaced and this allows the quantum dot to emit photons containing less energy, i.e. those with longer wavelengths. Quantum dots must absorb at a higher energy level than they emit and size scales with color within a given material system. For example, for CdSe quantum

dots, which emits in the visible, the larger the dots, the more red-shifted the emission is, and the smaller the dots, the more blue-shifted the emission is. (Figure 28) In other quantum dot systems (such as InN or GaN), the dots may emit outside the visible region, for instance in the IR or UV regions. Therefore, it is important to only compare size and color within a given material system. The size and shape of the quantum dot is determined during synthesis and is based on temperature, time, and the ligands attached (90, 94). This ability to tune the size of quantum dots is highly advantageous, especially in the imaging world.

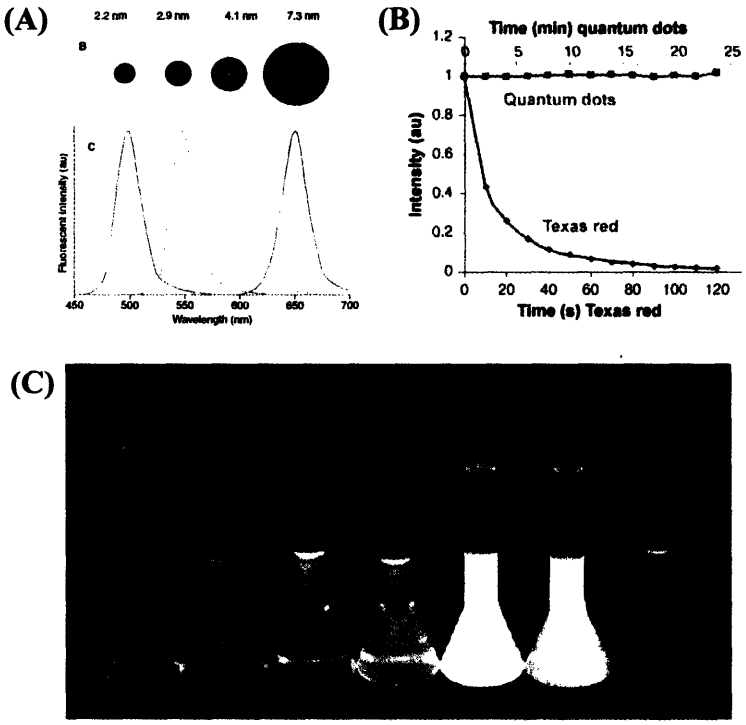

Figure 28. Quantum Dot Characteristics. **(A)** Relative sizes and emission wavelengths of various quantum dots (95) **(B)** Graph comparing the photo-bleaching of quantum dots and organic dyes (96) **(C)** Fluorescence induced by exposure to ultraviolet light in vials containing various sized Cadmium Selenide (CdSe) quantum dots. (Courtesy of Dr. D. Talapin, University of Hamburg, http://www.chemie.uni-hamburg.de/pc/Weller/).

Quantum dots are already being used in biological research and in medicine. (Figure 29) They have been used in visualizing DNA microarrays (90, 97), in labeling cells and tissues (90), and in

staining proteins, microtubules, and actin (90, 98). Quantum dots have been used in vascular imaging, where these dots have a longer lifetime in the body as compared to organic dyes (95). Quantum dots have been applied toward cell detection, cell tracking and lineage determination (90), as well as toward recognizing DNA sequences by distinguishing two difference sequences with two different colored quantum dots (95). Quantum dots have also been injected and used as a surgical guide to reduce the size of the incision necessary and to keep track of the site after surgery (99).

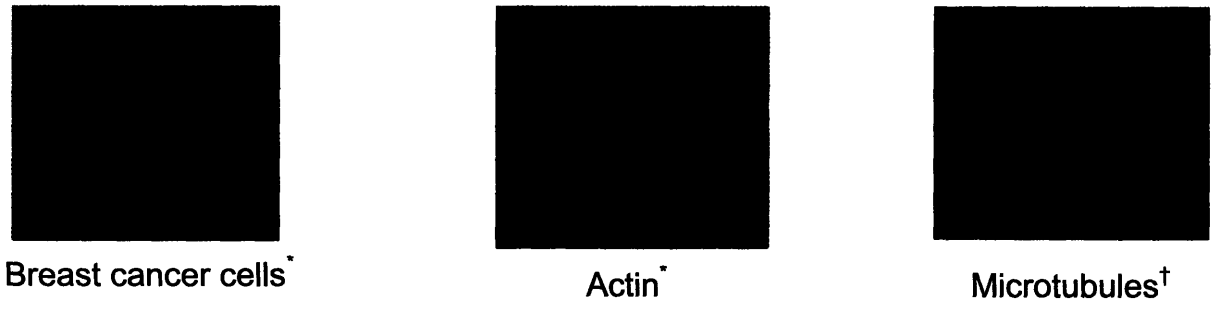

Figure 29. Uses of Quantum Dots in Biological Imaging. †Reprinted with permission from (95). Copyright (2006) Future Drugs. * Reprinted with permission from (96). Copyright (2005) Future Drugs.

For the purpose of detecting cancer lesions, in the case of breast cancer, quantum dots attached to phage, that are targeted to lesions on a biopsy, can be visualized using a fluorescent microscope and camera.

As with any foreign body, there is also the question of cytotoxicity. And with the current Cadmium Selenide quantum dots, there are problems of toxicity due to release of Cd^{2+} or Se^{2-} ions (90, 100), where free Cd^{2+} is cytotoxic (100). In many studies, it was shown that surface oxidation can occur from a combined aqueous/UV excitation. (101) This can lead to release of Cd^{2+} ions. To address this problem, current approaches to this problem include coating the CdSe

core with a shell layer that serves as a barrier to oxygen diffusion. A common shell being used is ZnS shell. However, in a combined aqueous/UV environment, even this barrier may not be enough to prevent oxidation and release of toxic ions. Therefore, more studies have to be done to determine necessary shell thickness as well as to find other material systems with less toxic components. In addition, studies have shown that protected quantum dots such as PEG-coated silanized quantum dots have negligible immune effect and do not activate genes involved in the immune or inflammatory process or heavy-metal-related toxicity (102). Currently, more toxicity studies are being done by labs here at MIT and elsewhere.

3.3.2.2 Magnetic Nanoparticle Basics

Magnetic nanoparticles form another subset of imaging tools that may be even more useful in terms of actual patient care because particles can be imaged from within a patient using Magnetic Resonance Imaging (MRI). A magnetic nanoparticle solution can be used as an MRI contrast agent and this has been tested successfully in mice (103). They can be synthesized with or without biomolecules such as trypsin (104). Particles assembled with biomolecules tend to agglomerate less and therefore be of smaller size. Currently, in the laboratory, several graduate students are synthesizing superparamagnetic iron oxide nanoparticles that are non-functionalized or functionalized with carboxyl or amine-terminated ends. These particles can be attached to the M13 virus platform to enable imaging.

3.3.2.3 Attaching CdSe/ZnS Quantum Dots to E3 Phage

Methods

Qdot 705 ITK amino (PEG) quantum dots were purchased from Invitrogen (Carlsbad, CA). The quantum dots were ZnS-coated CdSe dots and had an average diameter of 15 nm. The ability to attach the nanoparticles to phage on a substrate was tested for their ability to be visualized by Atomic Force Microscopy (AFM, Digital Instruments, Dimension 3100) in tapping mode under dry conditions. E3S1 phage (E3 on p8, streptavidin binding-motif on p3, 50 µl, 10^7 pfu/µl) was deposited on a silicon wafer, incubated at room temperature for 30 minutes, rinsed with 100 µl water, dried under vacuum, and then imaged on AFM. Quantum dots (50 µl, 0.8 nM in TBS) were then added to the phage-coated wafer and incubated for 1 hr at room temperature. The wafer was then rinsed with 100 µl water and imaged with AFM.

Results and Discussion

Figure 30 shows E4S1 phage deposited on silicon wafer and Figure 31 shows the addition of ZnS-coated CdSe quantum dots to the phage on silicon. AFM images before and after adding quantum dots show stark differences, especially in the phase image. The amine-terminated dots show affinity for the phage and attach to the negatively charged E3S1 phage preferentially, as shown by the many dots along the phage surface in Figure 31, while Figure 30 shows bare phage, without the rough appearance rendered by the dots.

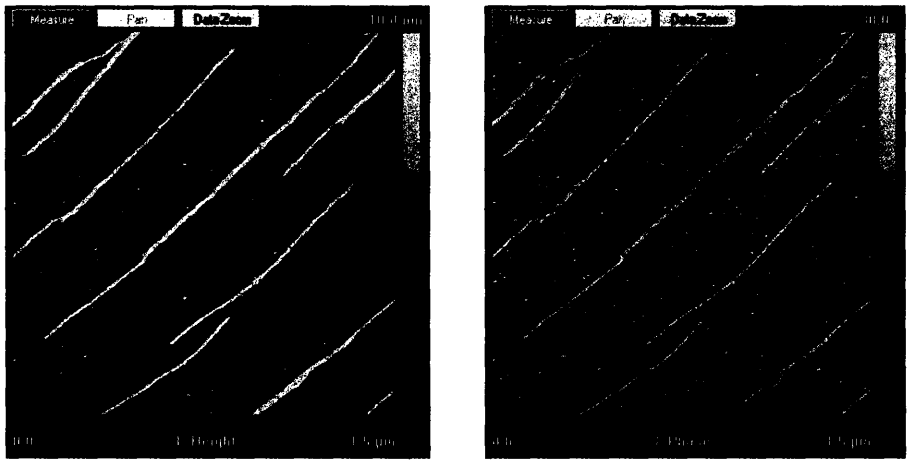

Figure 30. E3S1 M13 Bacteriophage on Silicon Wafer. E3S1 phage (50 ul, 10^7 pfu/µl) was deposited on silicon wafer. Analyzed by AFM.

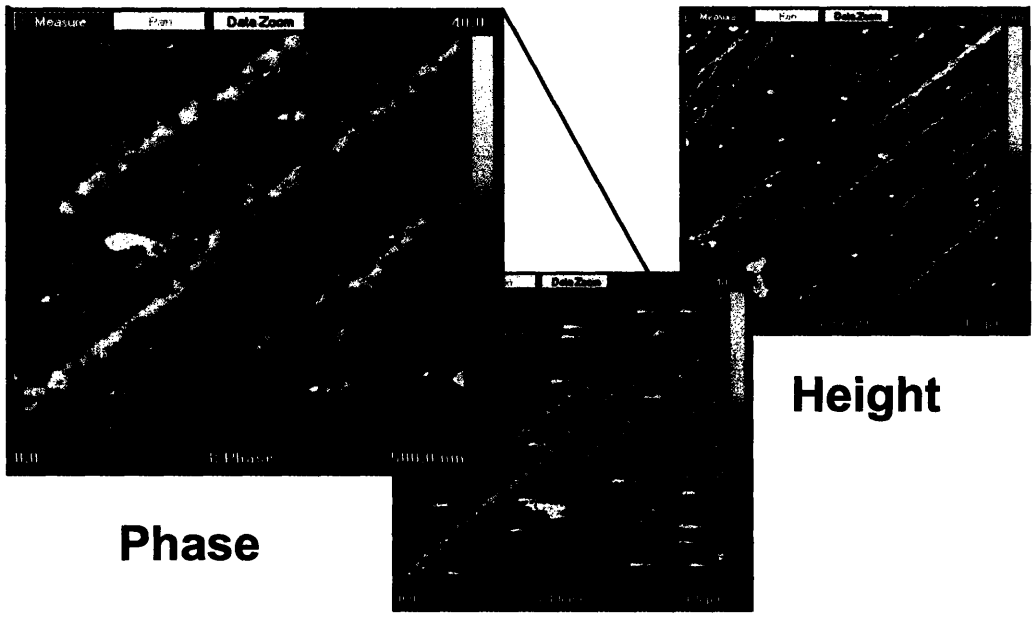

Figure 31. E3S1 M13 Bacteriophage Coated with Amine-Terminated CdSe/ZnS Quantum Dots. Quantum dots (50 ul, 0.8nM in TBS) were added to the phage on silicon and rinsed with water and imaged with AFM.

The sticking of the quantum dots to the phage shows that the amine terminated ZnS-coated CdSe quantum dots are capable of attaching to E3S1 phage if the phage is on a surface. However, since ultimately, the phage-nanoparticle cancer detection platform would be injected as a

solution, additional experiments would have to be done to see if the quantum dots can attach to E3S1 phage in solution.

3.3.2.4 Ways to Water Solubilize Nanoparticles

Background

Nanoparticles are generally synthesized in organic solvents, and in order for them to be compatible with *in vivo* use, they have to be water solubilized. There are many methods of solubilizing nanoparticles that have been continuously developed by researchers. For example, one method of solubilization is by manipulating hydrophobic interactions. In other words, one can intercalate an amphiphilic molecule with the hydrophobic surfactant covering the quantum dots following the synthesis steps (105).

One example of the hydrophobic interaction between the amphiphilic molecule and the surfactant coating the quantum dots is the use of poly(ethylene glycol) (PEG) as the amphiphilic molecule (106). (Figure 32) The advantage to this system for *in vivo* work is that PEG is not immunogenic or antigenic and can prevent biomolecule adhesion.

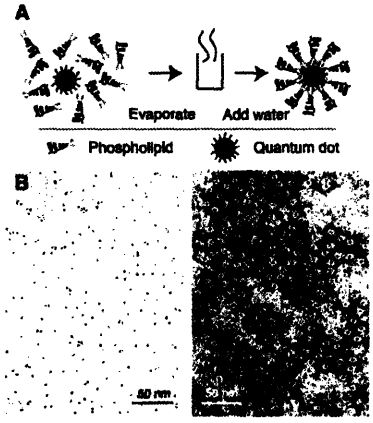

Figure 32. 4-nm ZnS coated CdSe QDots in Phospholipid Block Co-Polymer Micelle. Reprinted with permission from (106). Copyright (2002) AAAS.

To have further flexibility in manipulating these nanoparticles, we can use bioconjugation techniques such as NHS-Maleimide chemistry (Figure 33) to attach peptides or various other moieties to our nanoparticles as need be.

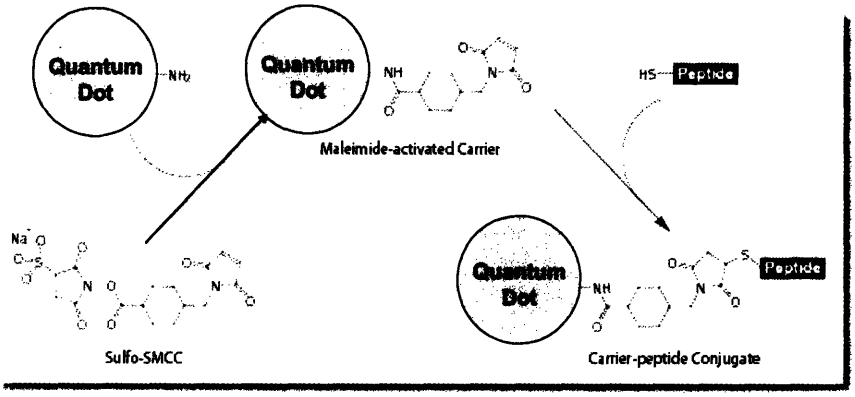

Figure 33. NHS-Maleimide Functionalizing of Quantum Dots. *Pierce*

3.3.2.5 GaN and InN Quantum Dots (In collaboration with Dr. Jifa Qi)

Background

While many of the commercial quantum dots are made from CdSe, in our laboratory, quantum dots from III-V semiconductor materials, such as GaN, InN, and InGaN, were synthesized. These materials are covalently bonded and have less of a chance of releasing toxic ions *in vivo*. GaN (bandgap = 3.4eV) emits in the UV region while InN (bandgap ~ 0.65eV) emits in infrared. So, if a mixture of InGaN can be formed, the emission can be tuned based on the ratio of Ga to In so that the entire spectrum from 365 nm to 1900 nm can be obtained. In addition, commercially available CdSe quantum dots require excitation by UV light in order to produce a signal. However, UV light can be harmful to cells, making CdSe dots infeasible for human imaging. However if InGaN quantum dots can be made to absorb in the visible and emit in the

IR, neither of which are wavelengths harmful to cells, this potentially creates an opportunity for completely safe *in vivo* imaging.

Methods

Synthesis of GaN and InN quantum dots were carried out by Jifa Qi. The quantum dots were coated with a surfactant upon synthesis, either Triocylphosphine Oxide (TOPO) or Hexadecyltrimethylammonium bromide (CTAB). Water solubilization of the dots was achieved using hydrophobic interactions with a set of amphiphilic polymers shown in Figure 34: 1,2-Dipalmitoyl-*sn*-Glycero-3-Phosphoethanolamine-N-[Methoxy(Polyethylene glycol)-2000] (DSPE-PEG(2000)), either 1,2-Distearoyl-*sn*-Glycero-3-Phosphoethanolamine-N-[Amino(Polyethylene Glycol)2000] (DSPE-PEG(2000)-Amino) or 1,2-Distearoyl-*sn*-Glycero-3-Phosphoethanolamine-N-[Carboxy(Polyethylene Glycol)2000] (DSPE-PEG(2000)-Carboxylic Acid), and 1,2-Dipalmitoyl-*sn*-Glycero-3-Phosphocholine (DPPC), all purchased from Avanti Polar Lipids (Alabaster, AL) as lyophilized powders.

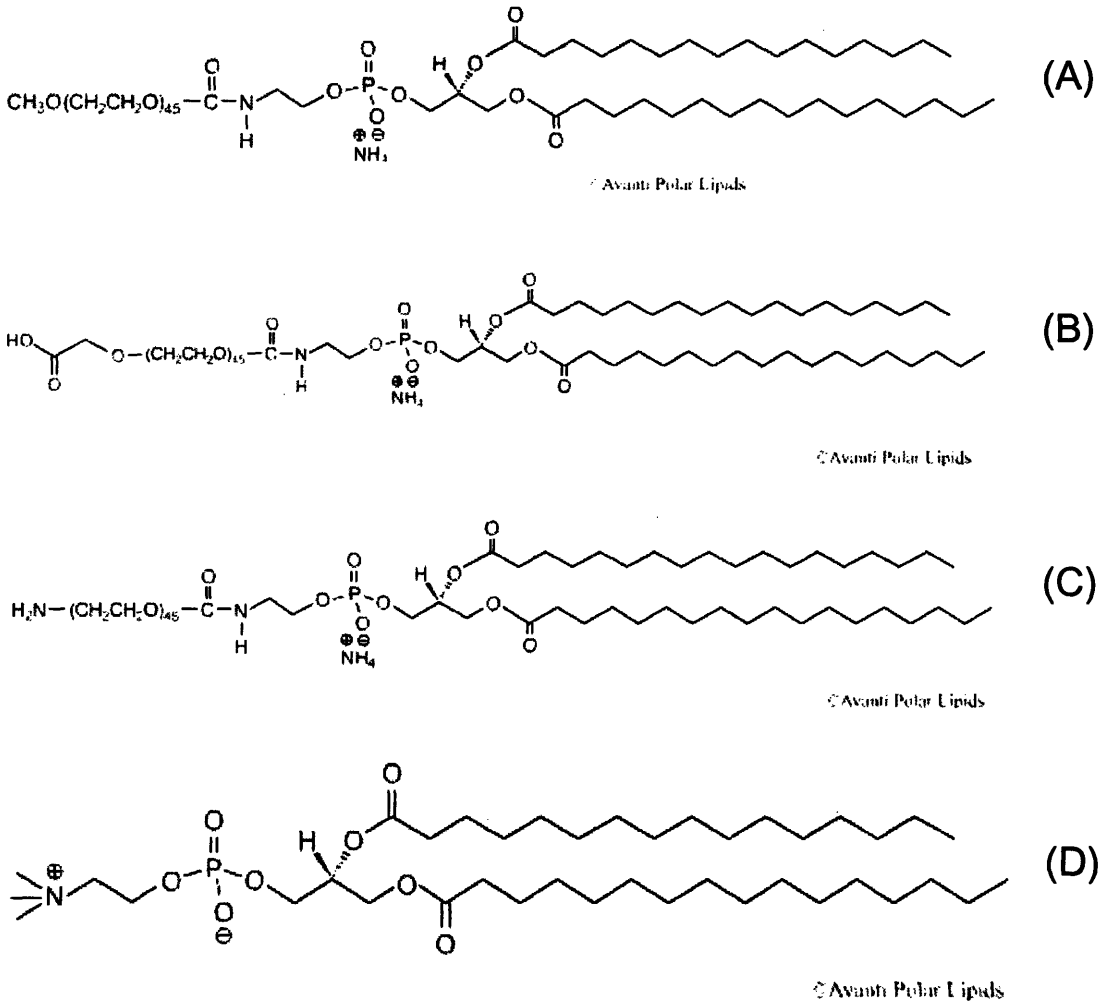

Figure 34. Amphiphilic Polymers Used to Water Solubilize GaN and InN Quantum Dots. **(A)** 1,2-Dipalmitoyl-sn-Glycero-3-Phosphoethanolamine-N-[Methoxy(Polyethylene glycol)-2000] (DSPE-PEG(2000)), either **(B)** 1,2-Distearoyl-sn-Glycero-3-Phosphoethanolamine-N-[Carboxy(Polyethylene Glycol)2000] (DSPE-PEG(2000)-Carboxylic Acid) or **(C)** 1,2-Distearoyl-sn-Glycero-3-Phosphoethanolamine-N-[Amino(Polyethylene Glycol)2000] (DSPE-PEG(2000)-Amine), and **(D)** 1,2-Dipalmitoyl-sn-Glycero-3-Phosphocholine (DPPC).

The procedure for solubilizing the quantum dots is outlined in Figure 35, using the amine terminated polymer as an example. All lipids were handled with a glass syringe and all chloroform solutions were kept in glass vials. A phospholipid mixture consisting of 60% DPPC, 20% DSPE-PEG(2000), and 20% DSPE-PEG(2000)-Amine by mass was dissolved in 0.5 ml of chloroform. GaN quantum dots (~20mg/ml) in 0.5 ml chloroform was also dissolved and then

added to the lipid mixture while vortexing the combined solution. The chloroform was evaporated overnight at room temperature followed by heating to 80°C and adding 1 ml water while mixing, forming a water soluble solution of GaN or InN quantum dots. To enhance miscibility, the mixture was sonicated on high for two hours and was purified via dialysis with Spectrapor 3 Membrane MWCO 3,500 for two hours to remove excess phospholipids.

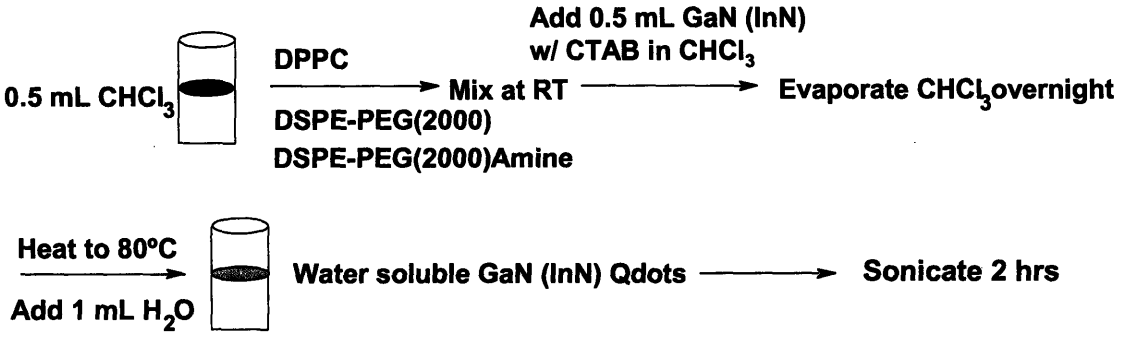

Figure 35. Schematic for Water Solubilizing GaN and InN Quantum Dots. A phospholipids mixture consisting of 60% DPPC, 20% DSPE-PEG(2000), and 20% DSPE-PEG(2000)-Amine by mass was dissolved in 0.5 ml of chloroform. GaN (~20mg/ml) in 0.5 ml chloroform was also dissolved and then added to the lipid mixture while vortexing the combined solution. The chloroform was evaporated overnight at room temperature followed by heating to 80°C and adding 1 ml water while mixing, forming a water soluble solution of GaN or InN quantum dots. To enhance miscibility, the mixture was sonicated on high for two hours and purified via dialysis with Spectrapor 3 Membrane MWCO 3,500 for two hours to remove excess phospholipids.

The first batch of quantum dots tests were GaN made with TOPO. Carboxy-terminated PEG was used for solubilization, while monitoring the change in zeta potential of the quantum dots before and after adding the phospholipids.

Amine functionalized phospholipids were also tested because of the ease of using fluorescamine to detect the number of amino termini as a comparative measure to zeta potential of how well-coated the quantum dots are.

Alternate surfactants, including CTAB, were employed during quantum dot synthesis to improve the solubility (measured by optical clarity of solution) of the dots.

A series of experiments was performed to determine the ratio of GaN to phospholipids for optimal solubility. Different proportions of GaN (CTAB) and phospholipids were used as well as a comparison of amine terminated PEG versus carboxylic acid terminated PEG as a solubilizer. GaN quantum dots (60 mg, made with CTAB) was added to 3 ml $CHCl_3$ and divided into six samples as indicated by Table 13. DSPE-PEG(2000) (14 mg), 8 mg DPPC, and 12 mg DSPE-PEG(2000)-Amine were mixed in 2 ml $CHCl_3$ and were divided into four samples as indicated in Table 13. Lastly, 6 mg DSPE-PEG(2000), 4 mg DPPC, and 6 mg DSPE-PEG(2000)-Carboxylic Acid were mixed in 1 ml $CHCl_3$ and divided among two samples (Table 10). All of the mixtures were evaporated at room temperature for 48 hours followed by heating at 80°C for 1 minute, then addition of 1 ml of 65°C water to the samples while vortexing. The samples were then all sonicated on high for 2 hours. They were stored at room temperature.

Table 10. Different Conditions of Water Solubilizing GaN Quantum Dots. 60mg of GaN(CTAB) was added to 3 ml $CHCl_3$ and divided into six amine samples. 14 mg DSPE-PEG(2000), 8 mg DPPC, and 12 mg DSPE-PEG(2000)-Amine were mixed in 2 ml $CHCl_3$ and were divided into 4 samples. Lastly, 6 mg DSPE-PEG(2000), 4 mg DPPC, and 6 mg DSPE-PEG(2000)-COOH were mixed in 1 ml $CHCl_3$ and divided between 2 samples.

Sample #	Condition	Vol. of Qdot Soln (ul)	Vol. of Phospholipid Soln (ul)
1	Amine - 10 mg/ml GaN	500	500
2	Amine - 10 mg/ml GaN - Sonicate GaN 15 min.	500	500
3	Amine - 8 mg/ml GaN	400	500
4	Amine - 12 mg/ml GaN	500	400
5	Carboxyl - 10 mg/ml GaN	500	500
6	Carboxyl - 12 mg/ml GaN	500	400

Indium Nitride (InN) was solubilized in much the same way. InN (30 mg) was added to 1.5 mL $CHCl_3$, vortexed, and mixed with a phospholipids solution of 6mg DPPC, 9mg DSPE-PEG(2000), and 9mg DSPE-PEG(2000)-Amine in 1.5 ml $CHCl_3$. The resultant solution was divided into three identical 1ml samples, allowed to evaporate overnight, then resuspended in

water and sonicated for 2 hours according to the procedure in Figure 35. The samples were purified via dialysis with Spectropor 3 Membrane MWCO 3,500 for 2 hours in distilled water and Transmission Electron Microscopy (TEM) samples were made and analyzed with a Jeol 2010 TEM with Energy Dispersive X-ray Analysis (EDX)

Results and Discussion

Figure 36 shows an illustration of the final quantum dots after coating with phospholipids.

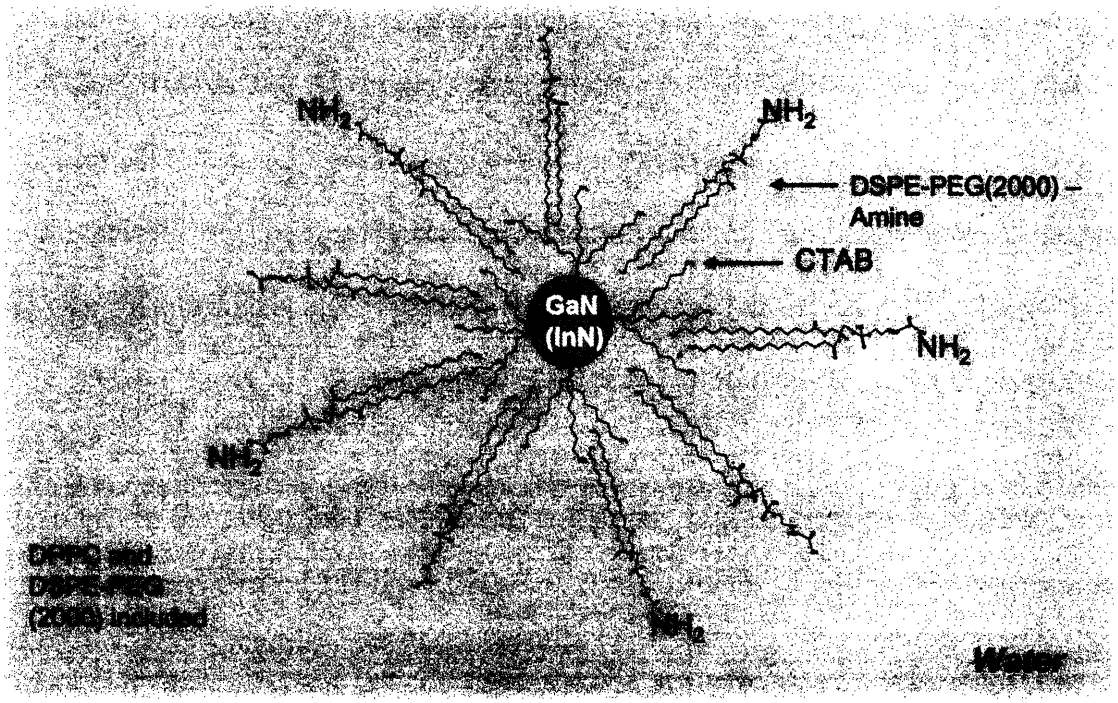

Figure 36. GaN or InN Quantum Dots Surrounded by Phospholipids. The phospholipids form an amphiphilic shell around the hydrophobic quantum dots, allowing the dots to be soluble in water.

Zeta potential measurements of GaN (TOPO) quantum dots with and without a phospholipids coat are shown in Table 11. Adsorbed TOPO layers would be positively charged (107) while the

carboxyl terminations would give a negative charge, so one would expect to see a change from positive to negative on the zeta potential.

Table 11. Zeta Potential Measurements of GaN (TOPO) Before and After Solubilizing with Phospholipids Containing Carboxyl Termini.

	Zeta Potential (mV)	Stdev	Mobility (m^2/Vs)	stdev
GaN (TOPO)	77.67	1.13	6.07	0.09
GaN (TOPO) + Phospholipids with carboxy termini	-46.01	1.02	-3.59	0.08

The results indicated a strong shift in charge of the quantum dots after coating with phospholipids. This outcome suggested that the quantum dots were coated with the phospholipids. While it is possible that the instrument was detecting free floating polymer clumps as well, since the measurement was averaged across the entire solution, such a large change in charge suggested that the quantum dots were well coated.

Results from the water solubilization experiment, using different ratios of GaN quantum dots and phospholipids are shown in Figure 37. Sample 1 remained clear, while Samples 2-6 were more translucent, bordering on opaque. Sample 4 looked the most opaque.

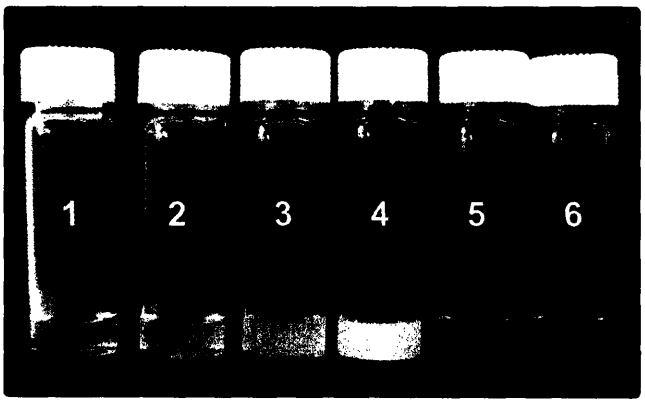

Figure 37. Water Solubilized GaN (CTAB). GaN (CTAB) samples upon adding phospholipids at different conditions (Table 10) to water solubilize the quantum dots.

The results of the ratio-determining experiment showed that the condition of 10mg/ml GaN, 3.5 mg/ml DSPE-PEG(2000), 2 mg/ml DPPC, and 3 mg/ml DSPE-PEG(2000)-Amine provided the best solubility among the conditions that were tested.

Water solubilization of InN resulted in a clear solution (Figure 38).

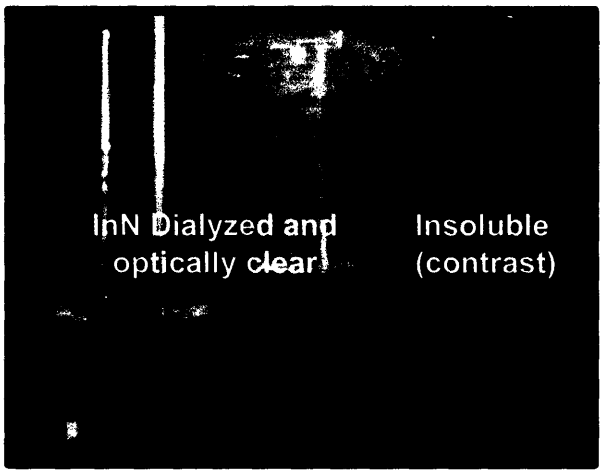

Figure 38. Water Soluble InN Quantum Dots. Comparison made with an insoluble solution (right) that is optically opaque.

TEM results are shown in Figure 39. EDX analysis show presence of an Indium peak and TEM images show quantum dots with diameters around 10 nm in small clusters. Lattice fringes were present, indicating the crystalline nature of the quantum dots.

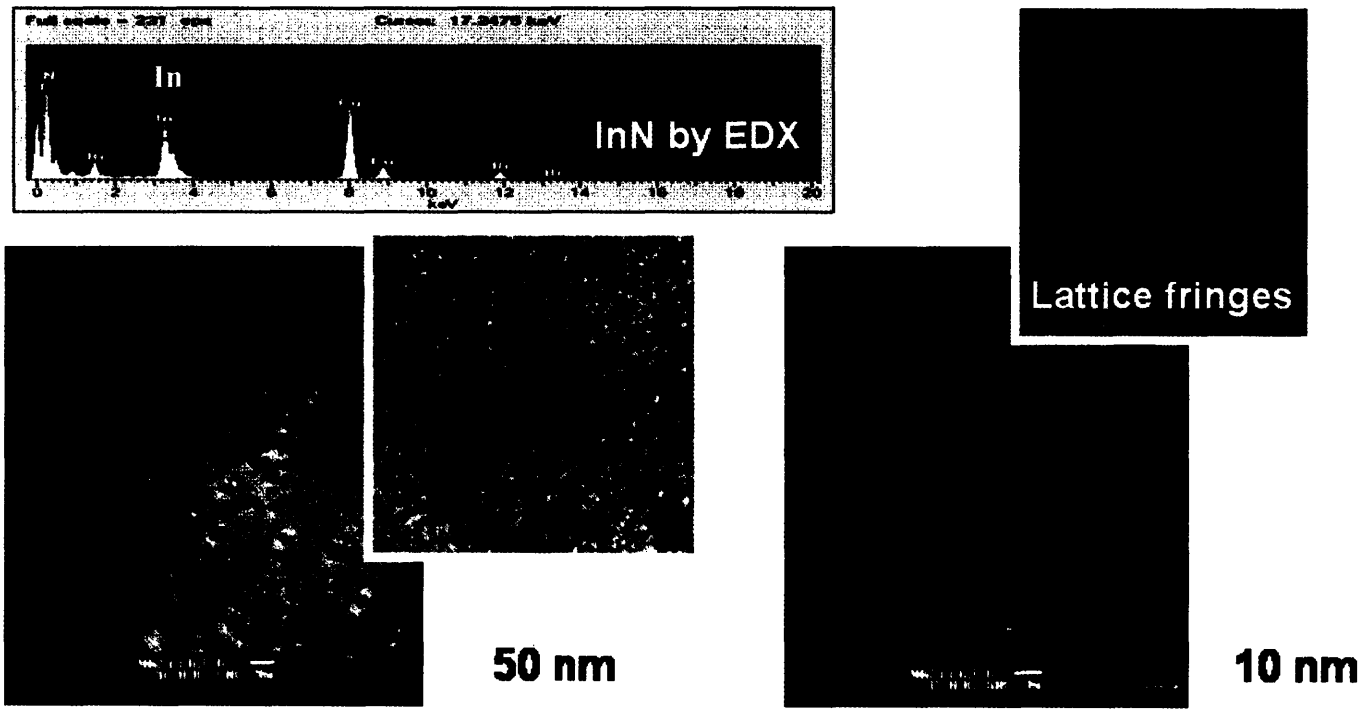

Figure 39. TEM with EDX Analysis of Water Solubilized InN. EDX analysis show presence of Indium peak and TEM images show quantum dots with diameters around 10nm in small clusters. Lattice fringes are present, indicating crystallinity of the quantum dots.

3.4 Conclusions and Future Work

The M13 bacteriophage presents many advantages for use in cancer detection due to its multifunctionality, avidity, and resistance to stress. In this chapter, we took a dual-prong approach, working simultaneously with genetic engineering of the M13 to insert cancer targeting peptides as well as working to solubilize and functionalize quantum dots and magnetic nanoparticles for attachment to phage. We were able to successfully create a p8 library as well as construct Type 83 phage with VCAM-1 targeting sequences on the p3 and a p8 capable of binding amine-terminated nanoparticles. Looking forward, for the detection of breast cancer, the p8 library can be used to biopan against VCAM-1. In addition, both amine-terminated magnetic

nanoparticles as well as amine-terminated quantum dots can be attached to the p8 or p3 of the M13 and visualized by fluorescent microscopy or MRI. The phage engineering work will be done in parallel with cell targeting, tumor targeting, and MRI testing at Massachusetts General Hospital.

Another important cancer target is colon cancer, which is the second leading cause of cancer-related death (after lung/bronchus cancer) in the United States. Colon cancer has a prolonged development period as polyps grow and eventually lead to cancer. Thus, good diagnostic technology is essential for the early detection of lesions so that polyps may be removed before they can progress to cancer. The current gold standard of diagnosis (colonoscopy) has a 20% miss rate (108) due to the limitation in sensitivity as lesion size decrease past 1 cm in diameter. The virus-based detection platform described above can be extended to the detection of colon cancer by insertion of a colon-cancer lesion targeting peptide, CPIEDRPMC,(109) into gIII. Additionally, it would be possible to biopan, using the p8 library, against colon cancer lesions for higher copy expression of the cancer targeting peptide, creating a high avidity interaction.

Lastly, another cancer of interest is prostate cancer. The Weissleder group has found a peptide sequence that can be cloned into the p3 or p8 and the same virus-based detection platform can be used to diagnose prostate cancer.

The ultimate goal is to have a versatile platform that combines imaging capabilities with specific targeting of cancer lesions that can be applied to a wide range of cancers with potential to extend to directed *in vivo* treatment.

CHAPTER 4 – Summary and Conclusions

The research discussed here demonstrated the use of the M13 bacteriophage in vaccine storage and cancer detection. For vaccine storage, a model protein, luciferase, was chosen to represent a protein based vaccine. Several peptides expressed on p3 of M13 that had affinity for luciferase were identified via phage display and two clones were amplified and combined with luciferase to form hybrid films. For cancer detection, there was a two prong approach. On the cancer targeting peptide engineering side, a p8 library was created, and a Type 83 phage with VCAM-1 expressed on the p3 and E3 on the p8 was engineered. On the nanoparticle side, GaN and InN quantum dots were successfully water solubilized, and CdSe/ZnS amine coated quantum dots were successfully attached to E3 phage on silicon substrate

For true incorporation into the medical areas, more work needs to be performed. For the vaccine project, there are several issues that need to be addressed, one of which is the major one of how to dissolve the film without threatening the integrity of the encapsulated protein. For the cancer project, the initial experiments shown here created a foundation for combining the cancer targeting peptides, quantum dots, and magnetic nanoparticles into a single system on top of the M13 bacteriophage, as well as a foundation for extending to other cancer systems such as prostate cancer, and colon cancer.

Appendix A: Biopanning Sequences

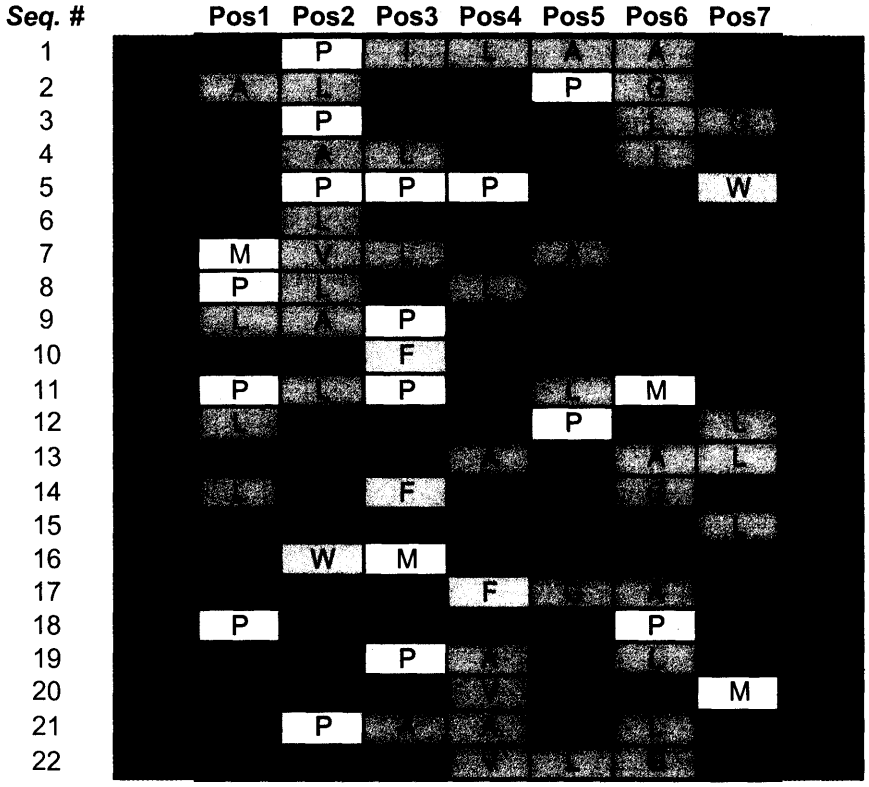

Figure A1. Biopanning Round 2 Eluted Peptide Sequences. The letters represent amino acids and the colors group them into categories based on their R groups: Acidic (Red), Basic (Blue), Hydrophobic (Orange), Hydroxyl (Green), Ring Groups (Tan), Proline (Yellow), Amide (Purple), and Methionine (White).

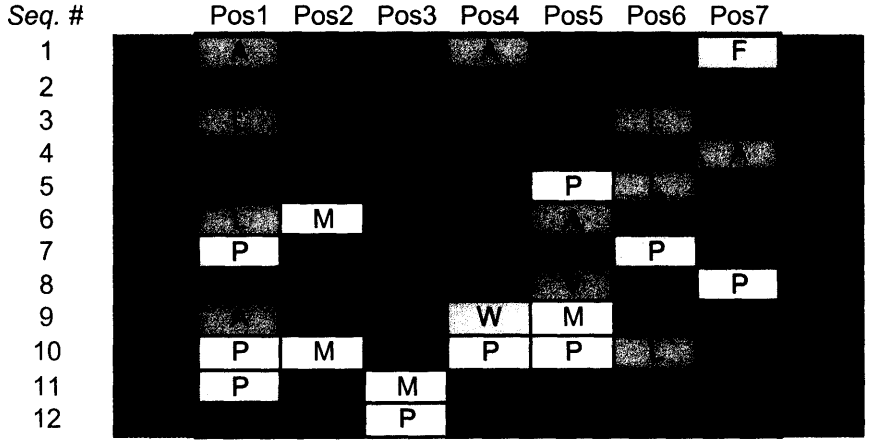

Figure A2. Biopanning Round 2b Eluted Peptide Sequences. The letters represent amino acids and the colors group them into categories based on their R groups: Acidic (Red), Basic (Blue), Hydrophobic (Orange), Hydroxyl (Green), Ring Groups (Tan), Proline (Yellow), Amide (Purple), and Methionine (White).

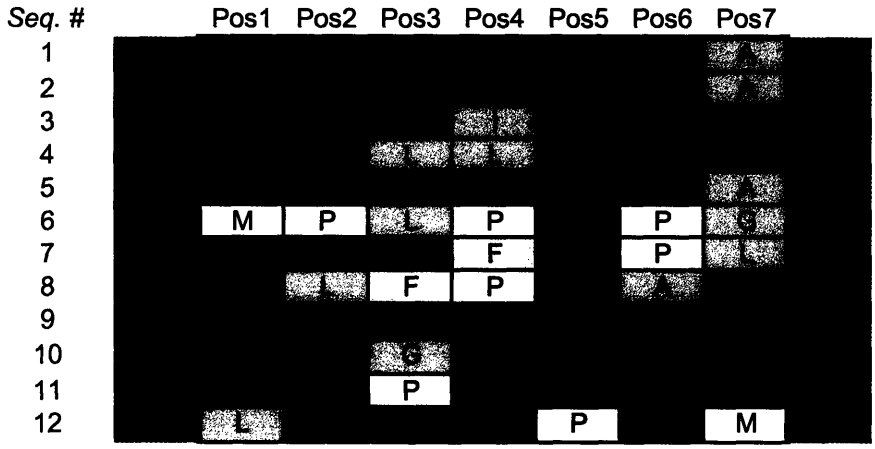

Figure A3. Biopanning Round 3b Eluted Peptide Sequences. The letters represent amino acids and the colors group them into categories based on their R groups: Acidic (Red), Basic (Blue), Hydrophobic (Orange), Hydroxyl (Green), Ring Groups (Tan), Proline (Yellow), Amide (Purple), and Methionine (White).

Appendix B: Human Phage Therapy References

Table B 1. Poland and Soviet Union Studies in Human Phage Therapy. (76)

Author(s)	Infection(s)	Etiologic agent(s)	Comments
Babalova et al.	Bacterial dysentery	*Shigella*	*Shigella* phages were successfully used for prophylaxis of bacterial dysentery.
Bogovazova et al.	Infections of skin and nasal mucosa	*K. ozaenae*, *K. rhinoscleromatis*, and *K. pneumoniae*	Adapted phages were reported to be effective in treating *Klebsiella* infections in all of the 109 patients.
Cislo et al.	Suppurative skin infections	*Pseudomonas*, *Staphylococcus*, *Klebsiella*, *Proteus*, and *E. coli*	Thirty-one patients having chronically infected skin ulcers were treated orally and locally with phages. The success rate was 74%.
Ioseliani et al.	Lung and pleural infections	*Staphylococcus*, *Streptococcus*, *E. coli*, and *Proteus*	Phages were successfully used together with antibiotics to treat lung and pleural infections in 45 patients.
Kochetkova et al.	Postoperative wound infections in cancer patients	*Staphylococcus* and *Pseudomonas*	A total of 131 cancer patients having postsurgical wound infections participated in the study. Of these, 65 patients received phages and the rest received antibiotics. Phage treatment was successful in 82% of the cases, and antibiotic treatment was successful in 61% of the cases.
Kucharewicz-Krukowska and Slopek	Various infections	*Staphylococcus*, *Klebsiella*, *E. coli*, *Pseudomonas*, and *Proteus*	Immunogenicity of therapeutic phages was analyzed in 57 patients. The authors concluded that the phages' immunogenicity did not impede therapy.
Kwarcinski et al.	Recurrent subphrenic abscess	*E. coli*	Recurrent subphrenic abscess (after stomach resection) caused by an antibiotic-resistant strain of *E. coli* was successfully treated with phages.
Litvinova et al.	Intestinal dysbacteriosis	*E. coli* and *Proteus*	Phages were successfully used together with bifidobacteria to treat antibiotic-associated dysbacteriosis in 500 low-birth-weight infants.
Meladze et al.	Lung and pleural infections	*Staphylococcus*	Phages were used to treat 223 patients having lung and pleural infections, and the results were compared to 117 cases where antibiotics were used. Full recovery was observed in 82% of the patients in the phage-treated group, as opposed to 64% of the patients in the antibiotic-treated group.
Miliutina and Vorotyntseva	Bacterial dysentery and salmonellosis	*Shigella* and *Salmonella*	The effectiveness of treating salmonellosis using phages and a combination of phages and antibiotics was examined. The combination of phages and antibiotics was reported to be effective in treating cases where antibiotics alone were ineffective.
Perepanova et al.	Inflammatory urologic diseases	*Staphylococcus*, *E. coli*, and *Proteus*	Adapted phages were used to treat acute and chronic urogenital inflammation in 46 patients. The efficacy of phage treatment was 92% (marked clinical improvements) and 84% (bacteriological clearance).
Sakandelidze and	Peritonitis,	*Staphylococcus*,	Phages administered subcutaneously or through surgical drains in

Meipariani	osteomyelitis, lung abscesses, and postsurgical wound infections	*Streptococcus*, and *Proteus*	236 patients having antibiotic-resistant infections eliminated the infections in 92% of the patients.
Sakandelidze	Infectious allergoses (rhinitis, pharyngitis, dermatitis, and conjunctivitis)	*Staphylococcus, Streptococcus, E. coli, Proteus*, enterococci, and *P. aeruginosa*	A total of 1,380 patients having infectious allergoses were treated with phages (360 patients), antibiotics (404 patients), or a combination of phages and antibiotics (576 patients). Clinical improvement was observed in 86, 48 and 83% of the cases, respectively.
Slopek et al.	Gastrointestinal tract, skin, head, and neck infections	*Staphylococcus, Pseudomonas, E. coli, Klebsiella*, and *Salmonella*	A total of 550 patients were treated with phages. The overall success rate of phage treatment was 92%.
Stroj et al.	Cerebrospinal meningitis	*K. pneumoniae*	Orally administered phages were used successfully to treat meningitis in a newborn (after antibiotic therapy failed).
Tolkacheva et al.	Bacterial dysentery	*E. coli* and *Proteus*	Phages were used together with bifidobacteria to treat bacterial dysentery in 59 immunosuppressed leukemia patients. The superiority of treatment with phage-bifidobacteria over antibiotics was reported.
Weber-Dabrowska et al.	Suppurative infections	*Staphylococcus* and various gram-negative bacteria	Orally administered phages were used to successfully treat 56 patients, and the phages were found to reach the patients' blood and urine.
Zhukov-Verezhnikov et al.	Suppurative surgical infections	*Staphylococcus, Streptococcus, E. coli*, and *Proteus*	The superiority of adapted phages (phages selected against bacterial strains isolated from individual patients) over commercial phage preparations was reported in treating 60 patients having suppurative infections.

Appendix C: M13SK Construction

(Adapted from SK Lee Doctoral Thesis (34))

M13SK phage vector was constructed for genetic engineering of both p3 and p8 by modifying M13KE phage vector (NEB) as described previously. T at position 1372 and C at position 1381 were mutated to A and G respectively by using overlap extension PCR (Figure C1).

Region from position 1179 to 1395 was amplified with primers 5'-M13KE-1179 (5'-GCTTGGTATAATCGCTGG-3') and 3'-M13KEmu-p8 (5'-GCTTTTGCGGGATC CTCACCC TCTGCAGCGAAAGACAG-3'). Region from position 1358 to 2277 was also amplified with primers 5'-M13KEmu-p8 (5'-CTG TCT TTC GCT GCA GAG GGT GAG GAT CCC GCA AAA GC-3') and 3'-M13KE-2 (5'-GAC AGG AGG TTG AGG CAG-3'). The amplified product of region from position 1179 to 2277 were obtained by performing additional PCR reaction with mixture of the two PCR products, 5'-M13KE-1179, and 3'-M13KE-2. The final PCR product and M13KE vector was digested by BspH I and Acc65 I, and ligated into M13KE vector. After transfection using XL1-Blue supercompetent cells (Stratagene), 100 μl of the cells were plated with 3ml of agarose top. Plaques were selected and sequenced to confirm the mutation. The *Pst* I site at position 6246 was deleted by mutating T to A at position 6250 by using same method. One PCR product were obtained with primer 5'-M13KE-5785 (5'-GTG GAC TCT TGT TCC AAA CTG-3') and 3'-M13KEmu-6250 (5'-CAG TGA ATT CGA GGA CCA GCA GGC ATG CAA GCT TG-3'), and the other PCR product were obtained with primer 5'-M13KEmu-6250 (5'-CAA GCT TGC ATG CCT GCT GGT CCT CGA ATT CAC TG-3') and3'-M13KE-7175 (5'-CAA TAA AGC CTC AGA GCA TAA AGC-3'). The two region was extended and

amplified with primer 5'-M13KE-5785 and 3'-M13KE-7175. The PCR product was digested with Hind III and Bgl II, and ligated into digested dsDNA of the mutant M13KE vector which contain mutation at p8 sites.

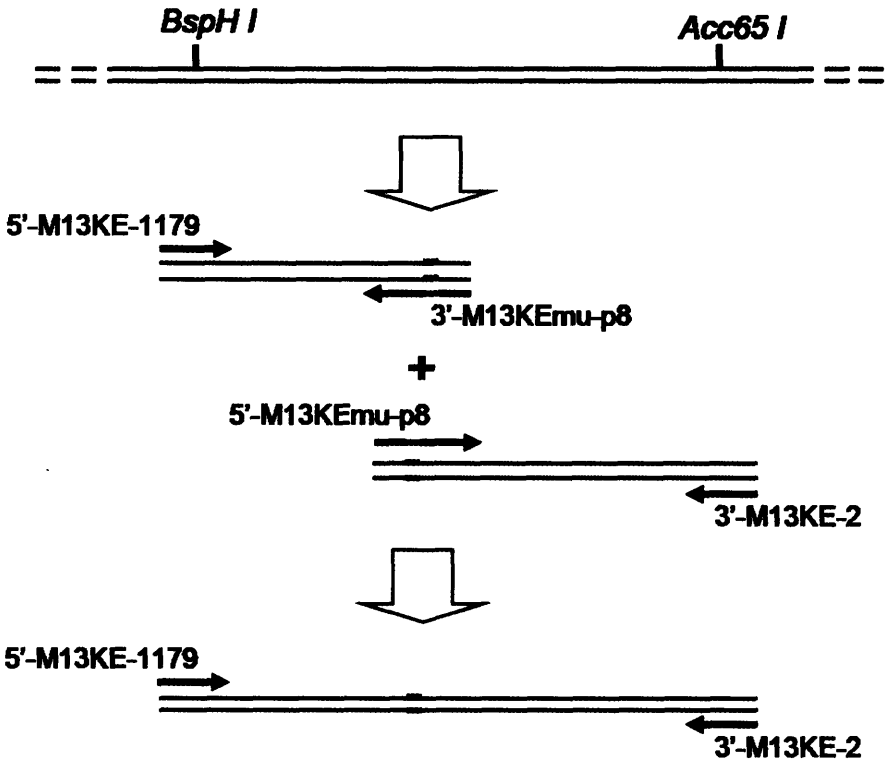

Figure C1. Overlap Extension PCR for pVIII Cloning Sites. Two individual PCR products with mutation sites were obtained. The two PCR products were extended and amplified with 5'-M13KE-1179 and 3'-M13KE-2 primers. (34)

Appendix D: M13SK P8 LIBRARY CONSTRUCTION

Detailed Protocol

Annealing:

2 PCR tubes
In each tube add: 35 ul EB Buffer
10 ul of 100uM Extension Primer
5 ul of p8 library oligo (50uM)
Total volume of 50ul

Thermocycler – Anneal_K
(95°C for 1 min, cycle down to 30°C at 0.1°/s) (takes about 15 minutes)

Extension:

4 PCR tubes

In each tube add: 25 ul annealed reaction
10 ul 10x Klenow Buffer (NEB Buffer2)
4ul of 10mM dNTP
2 ul of Klenow Fragment (10U/ul)
59 ul of H20
Total volume of 100ul

Thermocycler – Extend
(37°C for 20 minutes (to extend) and 75°C for 20 min (heat inactivation of klenow fragment))

QiaEx II Gel Extraction (Desalt and Concentrate DNA)

- Transfer each extension solution to 1.5ml Eppendorf
- Add 6 volumes (600ul) of Buffer QX1 (for <100bp)
- Vortex QiaExII beads well for 30 seconds
- Add 15 ul QiaExII beads to each sample
- Incubate 10 min RT mixing every 2 minutes by hand
- Centrifuge 13,000 rpm 30 seconds
- Remove supernatant and dispose
- Wash pellet with 500ul of Buffer PE and can combine 2 samples at a time
- Spin, then repeat wash, spin

- Remove supernatant well!
- Airdry 20-25 minutes (until see it's dried – a bit white)
- Add 20 ul EB Buffer to resuspend pellet
- Incubate 5 minutes RT
- Spin
- Take supernatant and transfer to new eppendorf and combine the 2 samples making 40 ul total
- Respin and retransfer

Check DNA concentration of extended oligo

Digestion of p8 Library Oligomer

Do on ice: (usually use 6 tubes)	Master Mix	
4 ul DNA	207.2 ul water	
4 ul BamHI Buffer	28 ul BamHI Buffer	Take 36 ul of master
29.6 ul Water	2.8 ul BSA	mix and add 4 ul
0.4 ul BSA	7 ul BamHI	library oligomer DNA
1 ul BamHI	7 ul Pst I	to it
1 ul Pst I		

Do master mixture!

37°C incubator 3 hours or overnight

Polyacrylamide Gel Purification (4-20% Novex TBE Gel)

- Make TBE buffer – dilute to 1X
- Wash gel container with Millipore water
- Pour in buffer first
- Take gels and open, strip off white sticker (probably need 2 gels)
- Load gel cassette with comb side up and notch facing inside
- Clamp
- Pour more buffer until filled past holes
- Take comb out and wash wells with buffer
- Make ladder: 10 ul of 25bp DNA ladder + 10 ul water + 4 ul loading dye (orange-G)
- Make samples: Add 8 ul of loading dye to each of the 40ul digested DNA samples
- Mix well
- Load samples (~24 ul for experimental samples and 12 ul for DNA ladders)
- Plug in gel device after put on lid
- Set voltage to 80V and run
- Takes about 100 minutes – just wait until yellow mark is in middle of last square
- When gel is done,
- Take a box, fill with water and add 2 ul ethidium bromide to it, mix

- Open up gel cassette with spatula
- Cut out whole gel and put into water with ethidium bromide
- Rock 10 minutes RT to stain the DNA
- Wash with water, and rock 3 minutes in Millipore water
- Image – make sure put some water on stage before sliding gel in
- Live/Focus, TransUV
- Take picture
- Cut out 27bp band and put 2 bands into each eppendorf tube
- Take picture of gel without band
- Elute DNA by adding 200ul of 100mM NaOAc pH4.5 1mM EDTA 1%SDS to each tube
- Shake 37°C overnight by putting eppendorfs into 14ml RB tubes

Digestion of Vector

Do on ice:	Master Mix	
20 ul Vector DNA	46.4 ul water	
11.6 ul water	16 ul BamHI Buffer	Take 20 ul and add
4 ul BamHI Buffer	1.6 ul BSA	20 ul DST RF (vector)
0.4 ul BSA	8 ul BamHI	
2 ul Pst I	8 ul Pst I	
2 ul BamHI		

(Do master mixtures)

37°C 3 hours or overnight

Purify eluted p8 Library Oligo using QiaExII Gel Extraction Kit

- Transfer all liquid from incubated DNA insert sample to new eppendorfs
- Add 1200 ul Buffer QX1
- Vortex beads well 30 seconds
- Add 10 ul beads and mix
- Incubate 10 minutes RT, mixing by hand every 2 minutes
- Centrifuge 1 minute, 13,000 rpm
- Remove supernatant
- Wash with 500 ul PE Buffer twice (include spin between washes)
- Airdry pellet 20-25 minutes until you see it dried (a bit white)
- Add 20 ul EB buffer and resuspend
- Incubate 5 minutes RT
- Centrifuge 30 seconds 13,000 rpm
- Transfer and respin
- Measure DNA concentration

Agarose Gel purification

- Make 2 batches of 0.8% agarose gel in 250ml Erlenmeyer :
- 40 mL TAE 1x Buffer + 0.32g Agarose
- Microwave with weight paper on top until all liquid and clear
- Cool down to RT (~ 5min)
- Add 2 ul ethidium bromide to agarose solution and mix well
- Pour agarose gel into tray – make sure the comb is in, clamp
- Get rid of bubbles, if any
- Let it set for ~ 20 minutes
- Put tray into gel machine and take out comb
- Pour 1X TAE buffer until cover
- Wash wells
- ***Making samples:***

  Add 4 ul loading dye to 20 ul ladder (1kb)
  Add 8 ul loading dye to the 40ul double digest samples
  Add 3 ul loading dye to 15 ul of vector uncut diluted 2x (7.5ul vector RF + 7.5ul water)
  Mix well
- 90V
- Runs about 55 minutes
- Image gel in holder
- Take photo
- Excise the 7kbp section for the single and double digest ; do not need the uncut circular vector
- Put each well section into separate eppendorf
- Weigh again and note the weight of the excised gel fragment

Extraction of DNA from Agarose using Qiaquick Gel Extraction Kit

- Take each eppendorf with excised vector and add 3x Buffer QG (ex. If 150mg section, add 450ul buffer QG)
- Incubate 10 minutes at 50C, vortexing every 2 minutes until agarose is dissolved
- Add 1x Isopropanol (ex. 150ul for 150mg sample), mix well
- Put solution into spin column – can do sequential addition and spin so as to concentrate
- Centrifuge 1 min 13,000 rpm
- Discard supernatant (can add 2nd sample to same column)
- Wash with 750ul Buffer PE twice, can wait 1 minute for each wash if wish
- Respin to get rid of residual PE buffer
- Put column in new 1.5ml eppendorf
- Add 50 ul Buffer EB to elute (20ul is the minimum recommended value)
- Incubate 1 minute RT
- Centrifuge 1 minute
- Measure DNA concentration of digested/purified vectors (DST , #9, or other vectors)

Ligation

Use following protocol if vector conc ~ 30ng/ul, insert conc ~ 20ng/ul.

For negative control, replace insert with 4 ul EB buffer

8 ul Vector (DST, #9, or other vector)
4 ul Insert
5 ul Water
2 ul T4 10x Buffer
1 ul T4 Ligase

(do master mix!)

16°C overnight

Electroporation of ligated vector/insert into electrocompetent cells

- Put 10 plates into 37C incubator
- Prepare 10 tubes of melted agarose in 14ml RB tubes (4 ml each)
- 12 ml of SOC into 37C incubator
- Prechill 10 sterile electroporation cuvettes
- Chill 10 sterile 1.5ml eppendorf tubes
- Thaw XL1 Electrocompetent cells

- Prepare electroporator – 1.7 kV
- Move 40 ul XL1 cells to each eppendorf
- Add 1 ul ligated DNA to cells, mix gently (done all on ice!)
- Incubate on ice 30 minutes
- Transfer cell-DNA mixture to a chilled electroporation cuvette, tap cuvette until mixture settles evenly to the bottom
- Pulse samples once and IMMEDIATELY add 960ul SOC medium and resuspend cells with pipet
- Transfer cells/DNA to sterile 14ml RB tube
- Incubate 30 minutes 37C shaker
- Plate 100ul
- Remaining 900 ul will be amplified
- Add 25 ml LB
  25 ul Tet
  to sterile 250ml flask and put in 37C shaking 4.5 hours

- Spin down bacteria 10 minutes 10,000rpm
- Move supernatant to new tube, respin 5 minutes
- New tube, add 1/6 volume of PEG/NaCl. Mix well
- Put in 4C overnight
- **Next Day:** spin Pegylated phage 13,000 rpm, 20 minutes, resuspend in 1ml TBS, transfer to eppendorf, respin down bacteria, re-PEG, incubate on ice > 60 minutes, spin down 13,000 15 minutes, resuspend in 200ul TBS, then titer it!

REFERENCES

1. Trun, N. & Trempy, J. (2004) *Fundamental Bacterial Genetics* (Blackwell Science, Malden, MA).

2. Abedon, S. (2000).

3. Karlsson, F., Malmborg-Hager, A. C., Albrekt, A. S., & Borrebaeck, C. A. K. (2005) **51,** 29.

4. Barbas III, C. F., Burton, D. R., Scott, J. K., & Silverman, G. J. (2001) *Phage Display - A Laboratory Manual* (Cold Spring Harbor Laboratory Press, Cold Spring Harbor, New York).

5. Blumer, K. J. & Steege, D. A. (1984) *Nucleic Acids Res.* **12,** 1847.

6. Steege, D. A. (2000) *RNA* **6,** 1079.

7. Hofschneider, P. H. & Preuss, A. (1963) *Journal of Molecular Biology* **20,** 450.

8. Rakonjac, J., Feng, J.-n., & Model, P. (1999) *Journal of Molecular Biology* **289,** 1253-1265.

9. Primrose, S. B. & Twyman, R. M. (2006) *Principles of Gene Manipulation and Genomics* (Blackwell Publishing, Malden, MA).

10. Huang, Y., Chiang, C. Y., Lee, S. K., Gao, Y., Hu, E. L., De Yoreo, J., & Belcher, A. M. (2005) **5,** 1429-1434.

11. Lee, S. K., Yun, D. S., & Belcher, A. M. (2006) *Biomacromolecules* **7,** 14-17.

12. Lee, S. W., Lee, S. K., & Belcher, A. M. (2003) *Adv Mater* **15,** 689.

13. Lee, S. W., Mao, C., Flynn, C. E., & Belcher, A. M. (2002) *Science* **296,** 892-895.

14. Lee, S.-W., Wood, B. M., & Belcher, A. M. (2003) *Langmuir* **19,** 1592-1598.

15. Mao, C., Flynn, C. E., Hayhurst, A., Sweeney, R., Qi, J., Georgiou, G., Iverson, B., & Belcher, A. M. (2003) *Proc.Natl.Acad.Sci.U.S.A.* **100,** 6946-6951.

16. Mao, C., Solis, D. J., Reiss, B. D., Kottmann, S. T., Sweeney, R. Y., Hayhurst, A., Georgiou, G., Iverson, B., & Belcher, A. M. (2004) *Science* **303,** 213-217.

17. Nam, K. T., Kim, D. W., Yoo, P. J., Chiang, C. Y., Meethong, N., Hammond, P. T., Chiang, Y. M., & Belcher, A. M. (2006) *Science* **312,** 885-888.

18. Nam, K. T., Peelle, B. R., Lee, S.-W., & Belcher, A. M. (2004) *Nano Letters* **4,** 23-27.

19. Peelle, B. R., Krauland, E. M., Wittrup, K. D., & Belcher, A. M. (2005) *Langmuir* **21,** 6929-6933.

20. Yoo, P. J., Nam, K. T., Qi, J., Lee, S. K., Park, J., Belcher, A. M., & Hammond, P. T. (2006) **5,** 234-240.

21. Fujita, S., Taki, T., & Taira, K. (2005) *Chembiochem* **6,** 315-321.

22. Kehoe, J. W. & Kay, B. K. (2005) *Chem. Rev.* **105,** 4056-4072.

23. Wang, L.-F. & Yu, M. (2004) *Current Drug Targets* **5,** 1-15.

24. Whaley, S. R., English, D. S., Hu, E. L., Barbara, P. F., & Belcher, A. M. (2000) *Nature* **405,** 665-668.

25. Lee, H. J., Zhang, Y., Zhu, C., Duff, K., & Pardridge, W. M. (2002) *J.Cereb.Blood Flow Metab.* **22,** 223-231.

26. Fairley, P. (2003) in *IEEE Spectrum*, pp. 36-41.

27. Arya, S. C. & Agarwal, N. (2004) *Acta Trop.* **90,** 223-225.

28. CDC (2003) in *Morbidity and Mortality Weekly Report* (Center for Disease Control, Atlanta, GA).

29. Weir, E. & Hatch, K. (2004) *Canadian Medical Association Journal* **171,** 1050.

30. Vajdy, M., Srivastava, I., Polo, J., Donnelly, J., O'Hagan, D., & Singh, M. (2004) *Immunol.Cell Biol.* **82,** 617-627.

31. Berzofsky, J. A., Ahlers, J. D., & Belyakov, I. M. (2001) *Nat.Rev.Immunol.* **1,** 209-219.

32. Dogic, Z. a. F., Seth (1997) *Physics Review Letters* **78,** 2417-2420.

33. Dogic, Z. & Fraden, S. (2000) *Langmuir* **16,** 7820.

34. Lee, S. K. (2006) (Massachusetts Institute of Technology, Cambridge, MA).

35. Branchini, B. R. (Tarbiat Modares University), p. 11.

36. Conti, E., Franks, N. P., & Brick, P. (1996) *Structure* **4,** 287-298.

37. Branchini, B. R., Magyar, R. A., Murtiashaw, M. H., Anderson, S. M., & Zimmer, M. (1998) *Biochemistry* **37,** 15311-15319.

38. Lee, J. & Timasheff, S. (1981) *J.Biol.Chem.* **256,** 7193-7201.

39. Carpenter, J. F. & Crowe, J. H. (1989) *Biochemistry* **28,** 3916.

40. Kim, Y. S., Jones, L. S., Dong, A., Kendrick, B. S., Chang, B. S., Manning, M. C., Randolph, T. W., & Carpenter, J. F. (2003) *Protein Sci.* **12,** 1252-1261.

41. Apantaku, L. M. (2000) *Am.Fam.Physician* **62,** 596-602, 605-596.

42. Summers, W. C. (1999) in *Felix d'Herelle and the Origins of Molecular Biology* (Yale University Press, New Haven, CT), p. 47.

43. Clark, J. R. & March, J. B. (2004) *Expert Review of Vaccines* **3,** 463-476.

44. Jepson, C. D. & March, J. B. (2004) *Vaccine* **22,** 2413-2419.

45. Clark, J. R. & March, J. B. (2006) *Trends Biotechnol.* **24,** 212-218.

46. Clark, J. R. & March, J. B. (2004) *FEMS Immunol.Med.Microbiol.* **40,** 21-26.

47. March, J. B., Clark, J. R., & Jepson, C. D. (2004) *Vaccine* **22,** 1666-1671.

48. March, J. B., Jepson, C. D., Clark, J. R., Totsika, M., & Calcutt, M. J. (2006) *Infect.Immun.* **74,** 167-174.

49. Funatsu, T., Taniyama, T., Tajima, T., Tadakuma, H., & Namiki, H. (2002) *Microbiology and Immunology* **46,** 365-369.

50. Goodridge, L., Chen, J., & Griffiths, M. (1999) *Applied and Environmental Microbiology* **65,** 1397-1404.

51. Kodikara, C. P., Crew, H. H., & Stewart, G. S. A. B. (1991) *FEMS Microbiology Letters* **83,** 261-265.

52. Watson, B. B. & Eveland, W. C. (1965) *The Journal Of Infectious Diseases* **115,** 363-369.

53. Petrenko, V. A. & Vodyanoy, V. J. (2003) *J.Microbiol.Methods* **53,** 253-262.

54. Emanuel, P., O'Brien, T., Burans, J., DasGupta, B. R., Valdes, J. J., & Eldefrawi, M. (1996) *Journal of Immunological Methods* **193,** 189-197.

55. Chan, S. W., Bye, J. M., Jackson, P., & Allain, J. P. (1996) *The Journal Of General Virology* **77** 2531-2539.

56. Plaisant, P., Burioni, R., Manzin, A., Solforosi, L., Candela, M., Gabrielli, A., Fadda, G., & Clementi, M. (1997) *Research in Virology* **148,** 165-169.

57. Williamson, R. A., Lazzarotto, T., Sanna, P. P., Bastidas, R. B., Dalla Casa, B., Campisi, G., Burioni, R., Landini, M. P., & Burton, D. R. (1997) *J. Clin. Microbio.* **35,** 247.

58. Muller, B. H., Chevrier, D., Boulain, J.-C., & Guesdon, J.-L. (1999) *Journal of Immunological Methods* **227,** 177-185.

59. Schmaljohn, C., Cui, Y., Kerby, S., Pennock, D., & Spik, K. (1999) *Virology* **258,** 189-200.

60. Maruyama, T., Rodriguez, L. L., Jahrling, P. B., Sanchez, A., Khan, A. S., Nichol, S. T., Peters, C. J., Parren, P. W., & Burton, D. R. (1999) *Journal Of Virology* **73,** 6024-6030.

61. Zhou, B., Wirsching, P., & Janda, K. D. (2002) *Proc.Natl.Acad.Sci.U.S.A.* **99,** 5241-5246.

62. Larocca, D., Burg, M. A., Jensen-Pergakes, K., Ravey, E. P., Gonzalez, A. M., & Baird, A. (2002) *Curr. Pharm. Biotechnol.* **3,** 45-57.

63. Larocca, D., Kassner, P. D., Witte, A., Ladner, R. C., Pierce, G. F., & Baird, A. (1999) *The FASEB Journal: Official Publication Of The Federation Of American Societies For Experimental Biology* **13,** 727-734.

64. Larocca, D., Witte, A., Johnson, W., Pierce, G. F., & Baird, A. (1998) *Human Gene Therapy* **9,** 2393-2399.

65. Hart, S. L., Knight, A. M., Harbottle, R. P., Mistry, A., Hunger, H. D., Cutler, D. F., Williamson, R., & Coutelle, C. (1994) *The Journal Of Biological Chemistry* **269,** 12468-12474.

66. Sperinde, J. J., Choi, S. J., & Szoka, F. C., Jr *The Journal Of Gene Medicine* **3,** 101-108.

67. Arap, W., Kolonin, M. G., Trepel, M., Lahdenranta, J., Cardo-Vila, M., Giordano, R. J., Mintz, P. J., Ardelt, P. U., Yao, V. J., Vidal, C. I., *et al.* (2002) *Nat.Med.* **8,** 121-127.

68. Kolonin, M. G., Sun, J., Do, K. A., Vidal, C. I., Ji, Y., Baggerly, K. A., Pasqualini, R., & Arap, W. (2006) *FASEB J.* **20,** 979-981.

69. Rajotte, D., Arap, W., Hagedorn, M., Koivunen, E., Pasqualini, R., & Ruoslahti, E. (1998) *The Journal Of Clinical Investigation* **102,** 430-437.

70. Petrenko, V. A., Smith, G. P., Gong, X., & Quinn, T. (1996) *Protein Eng.* **9,** 797-801.

71. Petrenko, V. A. & Smith, G. P. (2000) *Protein Eng.* **13,** 589-592.

72. Petrenko, V. A. & Sorokulova, I. B. (2004) *J.Microbiol.Methods* **58,** 147-168.

73. Pirisi, A. (2000) *The Lancet* **356,** 1418.

74. Bruttin, A. & Brussow, H. (2005) *Antimicrob.Agents Chemother.* **49,** 2874-2878.

75. Carrera, M. R., Kaufmann, G. F., Mee, J. M., Meijler, M. M., Koob, G. F., & Janda, K. D. (2004) *Proc.Natl.Acad.Sci.U.S.A.* **101,** 10416-10421.

76. Sulakvelidze, A., Alavidze, Z., & Morris, J. G., Jr. (2001) *Antimicrob.Agents Chemother.* **45,** 649-659.

77. Holliger, P., Riechmann, L., & Williams, R. L. (1999) *Journal of Molecular Biology* **288,** 649-657.

78. Olofsson, L., Ankarloo, J., Andersson, P. O., & Nicholls, I. A. (2001) *Chemistry & Biology* **8,** 661-671.

79. Krag, D. N., Shukla, G. S., Shen, G.-P., Pero, S., Ashikaga, T., Fuller, S., Weaver, D. L., Burdette-Radoux, S., & Thomas, C. (2006) *Cancer Res* **66,** 7724-7733.

80. Merril, C. R., Biswas, B., Carlton, R., Jensen, N. C., Creed, G. J., Zullo, S., & Adhya, S. (1996), pp. 3188-3192.

81. Imaginis (2006) (Imaginis Corp.), p. 2.

82. Kolb, T., Lichy, J., & Newhouse, J. (1998) *Radiology* **207,** 191-199.

83. Gutman, M. & Fidler, I. J. *World Journal Of Surgery* **19,** 226-234.

84. Menger, M. D. & Vollmar, B. (1996) *The British Journal Of Surgery* **83,** 588-601.

85. Minn, A. J., Gupta, G. P., Siegel, P. M., Bos, P. D., Shu, W., Giri, D. D., Viale, A., Olshen, A. B., Gerald, W. L., & Massague, J. (2005) *Nature* **436,** 518-524.

86. Fidler, I. J. (2003) *Nature Reviews Cancer* **3,** 453-458.

87. Solomayer, E. F., Diel, I. J., Meyberg, G. C., Gollan, C., & Bastert, G. (2000) *Breast Cancer Res.Treat.* **59,** 271-278.

88. O'Hanlon, D. M., Fitzsimons, H., Lynch, J., Tormey, S., Malone, C., & Given, H. F. (2002) *Eur.J.Cancer* **38,** 2252-2257.

89. Kelly, K. A., Allport, J. R., Tsourkas, A., Shinde-Patil, V. R., Josephson, L., & Weissleder, R. (2005) *Circ Res* **96,** 327-336.

90. Michalet, X., Pinaud, F. F., Bentolila, L. A., Tsay, J. M., Doose, S., Li, J. J., Sundaresan, G., Wu, A. M., Gambhir, S. S., & Weiss, S. (2005) *Science* **307,** 538-544.

91. Ballou, B., Lagerholm, B. C., Ernst, L. A., Bruchez, M. P., & Waggoner, A. S. (2004) *Bioconjug.Chem.* **15,** 79-86.

92. Chan, W. C. (1998) *Science* **281,** 2016-2018.

93. Dahan, M., Laurence, T., Pinaud, F., Chemla, D. S., Alivisatos, A. P., Sauer, M., & Weiss, S. (2001) *Optics Letters* **26,** 825.

94. Alivisatos, A. (1996) *Science* **271,** 933-937.

95. Smith, A. M., Dave, S., Nie, S., True, L., & Gao, X. (2006) *Expert Review of Molecular Diagnostics* **6,** 231-244.

96. Gao, X., Yang, L., Petros, J. A., Marshall, F. F., Simons, J. W., & Nie, S. (2005) *Curr.Opin.Biotechnol.* **16,** 63-72.

97. Alivisatos, P. (2004) *Nat.Biotechnol.* **22,** 47-52.

98. Wu, X., Liu, H., Liu, J., Haley, K. N., Treadway, J. A., Larson, J. P., Ge, N., Peale, F., & Bruchez, M. P. (2003) *Nat.Biotechnol.* **21,** 41-46.

99. Green, M. (2004) *Angew.Chem.Int.Ed Engl.* **43,** 4129-4131.

100. Derfus, A. M., Chan, W. C. W., & Bhatia, S. N. (2004) *Nano Lett* **4,** 11-18.

101. Ozkan, M. (2004) *Drug Discovery Today* **9,** 7.

102. Zhang, T., Stilwell, J. L., Gerion, D., Ding, L., Elboudwarej, O., Cooke, P. A., Gray, J. W., Alivisatos, A. P., & Chen, F. F. (2006) *Nano Letters* **6,** 800-808.

103. Kim, D. K., Zhang, Y., Voit, W., Rao, K., Kehr, J., Bjelke, B., & Muhammed, M. (2001) *Scr.Mater.* **44,** 1713 -1717.

104. Kim, T., Reis, L., Rajan, K., & Shima, M. (2005) *Journal of Magnetism and Magnetic Materials* **295,** 132-138.

105. Pellegrino, T., Manna, L., Kudera, S., Koktysh, T. L. D., Rogach, A. L., Keller, S., Radler, J., Natile, G., & Parak, W. J. (2004) *Nano Letters* **4,** 703-707.

106. Dubertret, B., Skourides, P., Norris, D. J., Noireaux, V., Brivanlou, A. H., & Libchaber, A. (2002) *Science* **298,** 1759-1762.

107. Jiang, J., Krauss, T. D., & Brus, L. E. (2000) *J. Phys. Chem. B* **104,** 11936-11941.

108. Rex, D. K., Cutler, C. S., Lemmel, G. T., Rahmani, E. Y., Clark, D. W., Helper, D. J., Lehman, G. A., & Mark, D. G. (1997) *Gastroenterology* **112,** 24-28.

109. Kelly, K., Alencar, H., Funovics, M., Mahmood, U., & Weissleder, R. (2004) *Cancer Res.* **64,** 6247-6251.